Laminin matrix adhesion regulates basal mammary epithelial cell identity

Englund, Johanna I; Bui, Hien; Dinç, Defne D; Paavolainen, Oona; McKenna, Tomás; Laitinen, Suvi; Munne, Pauliina; Klefström, Juha; Peuhu, Emilia; Katajisto, Pekka

The Company of
Biologists

RESEARCH ARTICLE

Laminin matrix adhesion regulates basal mammary epithelial cell identity

Johanna I. Englund[1], Hien Bui[1], Defne D. Dinç[2,3], Oona Paavolainen[2,3], Tomás McKenna[4], Suvi Laitinen[1], Pauliina Munne[5], Juha Klefström[5], Emilia Peuhu[2,3] and Pekka Katajisto[1,4,6,*]

ABSTRACT

Mammary epithelium is a bilayered ductal network composed of luminal and basal epithelial cells, which together drive the growth and functional differentiation of the gland. Basal mammary epithelial cells (MECs) exhibit remarkable plasticity and progenitor activity that facilitate epithelial expansion. However, their activity must be tightly regulated to restrict excess basal cell activity. Here, we show that adhesion of basal cells to laminin α5-containing basement membrane matrix, which is produced by luminal cells, presents such a control mechanism. Adhesion to laminin α5 directs basal cells towards a luminal cell fate, and thereby results in a marked decrease of basal MEC progenitor activity *in vitro* and *in vivo*. Mechanistically, these effects are mediated through β4-integrin and activation of p21 (encoded by *CDKN1A*). Thus, we demonstrate that laminin matrix adhesion is a key determinant of basal identity and essential to building and maintaining a functional multicellular epithelium.

KEY WORDS: Mammary epithelium, Progenitor activity, Cell identity, Adhesion, Extracellular matrix, Basement membrane, Laminin

INTRODUCTION

Mammary epithelial lineages develop during embryogenesis from multipotent basal keratin-14 (K14)-positive progenitors, whereas in post-natal epithelium, luminal and basal epithelial cells are generated from specified unipotent luminal and basal progenitors (Lilja et al., 2018; Van Keymeulen et al., 2011; Wuidart et al., 2018). Basal mammary epithelial cells (MECs) have been shown to display high progenitor activity and plasticity, or the ability to alter their identity, as demonstrated by their capability to form a functional mammary epithelium consisting of both luminal and basal lineages in mammary reconstitution assays (Shackleton et al., 2006; Stingl et al., 2006; Van Keymeulen et al., 2011). Basal cells can also replace luminal cells *in vivo* after injury or genotoxic stress by reactivating multipotency (Centonze et al., 2020; Seldin and Macara, 2020). These data illustrate that basal MECs exhibit extraordinary plasticity, especially during regeneration and repair,

to ensure proportionate growth of the mammary epithelium. In contrast, when basal cell multipotency and plasticity are not required, such properties must be tightly controlled to preserve the functionality of the tissue.

Paracrine and hormonal factors have been shown to mediate crosstalk between the epithelial layers to regulate growth and differentiation of the mammary epithelium and the basal MEC plasticity (Asselin-Labat et al., 2010; Cai et al., 2014; Centonze et al., 2020; Englund et al., 2021; Forster et al., 2014; Macias and Hinck, 2012; Rajaram et al., 2015). Additionally, the structural microenvironment, including extracellular matrix (ECM) and basement membrane (BM), control the growth and function of the mammary epithelium (Gudjonsson et al., 2002; Maller et al., 2010; Nerger et al., 2021). Especially laminins, proteins essential for BM formation, have been shown to critically regulate progenitor cell function of various tissues *in vivo* and *in vitro* (LaBarge et al., 2009; Rodin et al., 2014). Given that both luminal and basal MECs contribute and adhere to the mammary ECM (Englund et al., 2021), it is plausible that specific ECM factors function as signals to and between the cell types. For instance, BM component laminin-111 (LM-111, comprising laminin α1, β1 and γ1 chains) produced by basal MECs regulates activity of the basal mammary progenitor cells (Gudjonsson et al., 2002; Inman et al., 2015; LaBarge et al., 2009), and downregulation of laminin-binding integrins β1, α3 or α6 leads to defects in epithelial growth and progenitor properties (Olabi et al., 2018; Romagnoli et al., 2020; Taddei et al., 2008). However, whether other laminin components in the mammary ECM regulate lineage-specific basal cell properties, including progenitor activity and plasticity, is not well understood. Recent data has shown that luminal MECs employ paracrine signals to control basal MEC characteristics (Centonze et al., 2020), which raises the possibility that luminal cells regulate basal cells and thereby maintain functional mammary tissue by also producing specific ECM constituents.

We recently demonstrated that the BM component laminin α5, which is expressed by the hormone receptor-positive (HR+) luminal epithelial cells, is essential for mammary gland development (Englund et al., 2021). In the absence of laminin α5 from the BM, the HR+ luminal epithelial cells fail to fully differentiate and support adjacent basal cells by paracrine secretion of Wnt4, leading to restrained growth of the entire epithelium. However, it remains unclear how adhesion to specific laminins affects basal MECs. Thus, we sought to uncouple the effect of laminin adhesion from the luminal MEC-driven epithelial growth, and to determine how adhesion to different laminins affects basal MEC properties including progenitor capabilities and plasticity. Here, we show that adhesion to laminin α5-containing laminin-521 (LM-521; comprising laminin α5, β2 and γ1 chains) matrix results in a marked decrease in progenitor activity of basal MECs *in vitro* and *in vivo*, accompanied by an activation of a luminal gene expression program. Furthermore, we show that decreased progenitor activity

1

and plasticity in basal MECs is attributed to suppression of the β1-integrin–phosphoinositide 3-kinase (PI3K) signaling axis, leading to activation of the self-renewal-controlling p21 (encoded by *CDKN1A*) pathway. Additionally, re-activation of PI3K or inhibition of p21 or β4-integrin, which we find is a critical regulator of p21, can rescue basal MEC progenitor activity irrespective of matrix adhesion. In conclusion, by using *in vitro* and *in vivo* model systems, we demonstrate that adhesion to specific laminin isoforms in the extracellular microenvironment has a regulatory role in mammary epithelial plasticity and lineage determination.

RESULTS

Luminal and basal MECs favor adhesion to their respective laminin matrix

We have previously shown that mouse luminal and basal MECs exhibit lineage-specific expression patterns of BM laminins (Englund et al., 2021). Luminal cells produce a majority of laminin α5, whereas basal cells produce a majority of laminin α1 and minute amounts of laminin α5 (Englund et al., 2021). To dissect whether adhesion to these laminins affects luminal and basal MEC

function differentially, we cultured basal human HMEC-FL2 cell line (Chaffer et al., 2011) or freshly isolated basal (CD29^{hi}/CD24$^+$) and luminal (CD29^{low}/CD24$^+$) mouse MEC (MMEC) populations on plates coated with recombinant LM-111 or LM-521 for 48 h to mimic BM adhesion (Fig. 1A; Fig. S1A,B). Interestingly, as detected by scanning electron microscopy (SEM) HMEC-FL2 cells grown on LM-111 had a more cuboidal morphology, whereas cells cultured on LM-521 were extensively flat (Fig. 1B). These observations hinted that MECs adhere to various laminins differentially, and therefore we assessed their cell adhesion dynamics by internal reflection microscopy (IRM) (Barr and Bunnell, 2009). Freshly isolated basal and luminal MECs were seeded on laminin coated plates and imaged directly after plating (Fig. 1C). Intriguingly, we observed that both cell types adhered to LM-521 more rapidly than to LM-111 (Fig. 1C). However, luminal MECs adhered to LM-521 faster than basal MECs, whereas basal MECs adhered to LM-111 faster than luminal cells. Comparably, HMEC-FL2s also initially adhered to LM-521 quicker than to LM-111 (Fig. S1C, Movies 1, 2). Furthermore, after 2 days in culture, the surface area occupied by single cells was larger on LM-521 than
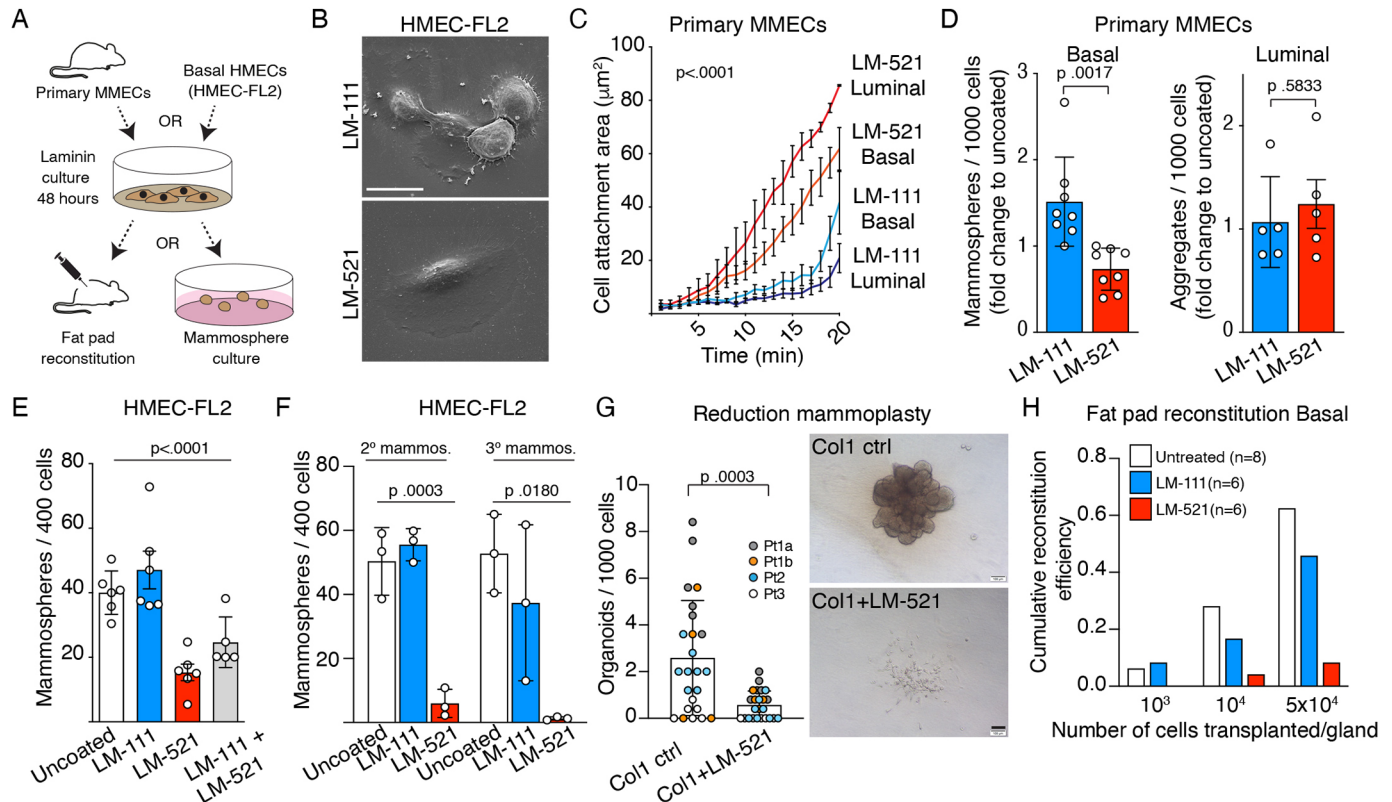

Fig. 1. Adhesion to specific laminin matrix regulates basal MEC progenitor activity. (A) Schematic showing the outline of the laminin pre-adhesion assay, where primary MMECs or HMEC-FL2s are cultured on 2D LM-111 or LM-521 matrix for 48 h prior to mammosphere culture or a fat pad reconstitution assay. (B) Scanning electron (SEM) micrographs of HMEC-FL2s grown on the indicated laminins. Images representative of three experiments. Scale bar: 20 μm. (C) Quantification of cell attachment area of primary MMECs using internal reflection microscopy (IRM) at indicated time points after seeding on indicated laminins. Data show mean±s.e.m., *n*=4 independent experiments. (D) Mammosphere or aggregate forming frequency of FACS sorted luminal and basal primary MMECs pre-adhered on the indicated laminins 14 days earlier. Basal cells *n*=8 and luminal cells *n*=5 independent experiments in both groups. (E) Mammosphere forming frequency of HMEC-FL2 cells pre-adhered to the indicated laminins or uncoated plastic. *n*=6 independent experiments, except for LM-111+LM-521 where *n*=5. (F) Secondary (2°) and tertiary (3°) mammosphere forming frequency of HMEC-FL2 cells initially pre-adhered to indicated laminins. *n*=3 independent experiments in all groups. (G) Organoid forming frequency of primary HMECs cultured in collagen I (Col I) and LM-521 or growth medium as control (ctrl). *n*=4 independent experiments from cells isolated from three patients. Representative images of growth in either condition. Scale bars: 100 μm. (H) Cumulative reconstitution efficiency of basal (CD29hi/CD24+) MMECs pre-adhered on LM-111 or LM-521 or untreated controls were transplanted into wild type hosts in indicated numbers. Efficiency was considered 1 if both transplanted glands of all the mice are 100% reconstituted. *n*=6 for LM-111 and LM-521 and *n*=8 for untreated group. All data show mean±s.d. from independent experiments unless otherwise stated. Unpaired two-tailed Student's *t*-test (D,F,G) or one-way ANOVA with Tukey's multiple comparison test (C,E) was used to compare indicated groups.

LM-111, which did not significantly differ from that of uncoated surface (Fig. S1D), yet the overall number of cells adhered in each condition did not significantly change (Fig. S1E). Thus, luminal and basal cells appear to preferentially adhere to the autologous laminin they produce, yet LM-521 provides a particularly adhesive substratum for both cell types.

Progenitor activity of mouse and human basal MECs is regulated by laminin adhesion *in vitro* and *in vivo*

Lineage-specific adhesion kinetics raised the possibility that distinct laminin adhesion could contribute to lineage-specific functions of basal MECs. The capability to form mammospheres is an attribute of basal MECs and an indicator of their progenitor cell activity *in vitro* (Dontu et al., 2003; Shaw et al., 2012). Hence, we pre-adhered primary basal MMECs and HMEC-FL2s to laminins for 48 h prior to mammosphere formation (Fig. 1A). The HMEC-FL2 cell line is derived from a CD44+ basal cell clone, which expresses basal markers including K14 and vimentin, and exhibits mammosphere-forming capabilities (Chaffer et al., 2011; Katajisto et al., 2015). Interestingly, LM-111 pre-adhesion increased mammosphere formation of primary basal MECs slightly compared to that seen on an uncoated surface (Fig. 1D), but in striking contrast, pre-adhesion on LM-521 decreased mammosphere formation significantly (Fig. 1D). However, luminal MECs formed non-spheroidal aggregates at a constant frequency irrespective of any pre-adhesion (Fig. 1D). Similarly, pre-adhesion of unsorted MECs or HMEC-FL2s to LM-521 decreased mammosphere formation substantially in comparison to that seen on uncoated plastic or LM-111 (Fig. 1E, Fig. S2A,B). Moreover, combining LM-111 and LM-521 during pre-adhesion did not significantly increase mammosphere formation compared to LM-521 alone (Fig. 1E), suggesting that LM-521 adhesion effects are dominant over LM-111. Additionally, the decrease in mammosphere formation after LM-521 pre-adhesion depended on the LM-521 concentration, but not on the duration of trypsinization (Fig. S2C,D). Furthermore, formation of secondary and tertiary HMEC mammospheres (Fig. 1F) was significantly reduced in cells initially adhered to LM-521, indicating a long-term reduction in their self-renewal capability. However, no difference in the mammosphere formation was observed when cultures were supplemented with soluble LM-111 or -521 (Fig. S2E). Thus, the observed effects occurred prior to mammosphere formation and required adhesion to a laminin-containing substratum. Also, no change in EdU positivity, cell number or apoptotic cells were observed between LM-111 and LM-521 cultures (Fig. S2F–H), suggesting that the laminin-induced differences in mammosphere formation reflect alterations in progenitor activity rather than proliferation or cell death. Taken together, these data indicate that adhesion to LM-521 induces long-term effects in the basal MEC self-renewal and progenitor activity *in vitro*.

Next, we investigated whether primary human MECs are similarly responsive to laminin adhesion. HMECs from reduction mammoplasties were plated into 3D collagen I gel culture with or without LM-521 (Fig. 1G). In contrast to the non-adherent mammosphere culture, collagen I gels provide an interstitial substratum allowing adhesion. This method was previously shown to allow assessment of the regenerative potential of primary human MECs (Linnemann et al., 2017), and to support formation of terminal ductal lobular unit (TDLU)-like branching structures when both basal and luminal cell types are present. In agreement, we observed formation of TDLU-like structures by control cells, while strikingly, the number of structures formed in the presence of

LM-521 was significantly decreased (Fig. 1G), suggesting that the regenerative potential of primary human MECs is diminished by LM-521 adhesion.

Finally, we performed mammary reconstitution assays to explore the *in vivo* effects of laminin pre-adhesion on progenitor activity. FACS-sorted basal and luminal MECs were pre-adhered on either LM-111 or LM-521 for 48 h and subsequently tested with a limiting-dilution reconstitution assay (Fig. 1H; Fig. S2I). Freshly isolated basal or luminal MMECs without pre-adhesion (untreated) served as controls (Fig. S2I). As expected, transplanting untreated basal cells resulted in outgrowths with increased frequency, whereas luminal cells yielded no outgrowths (Fig. 1H, Fig. S2I). Also, as shown previously, preadhesion resulted in lower reconstitution rates than untreated cells (Welm et al., 2008) (Fig. 1H). However, LM-111 pre-adhered basal cells formed outgrowths more often than LM-521 pre-adhered basal cells (Fig. 1H, Fig. S2I), with progenitor cell frequencies of 1/39996 in LM-111 compared to 1/102287 in LM-521 estimated using the extreme limiting dilution assay (Hu and Smyth, 2009). Consequently, adhesion to specific laminin isoforms can critically modulate tissue reconstitution capability of basal MECs. Furthermore, LM-521 pre-treatment reduced the reconstitution potential of basal MECs even when transplanted together with luminal MECs (Fig. S2J), indicating that LM-521 adhesion impedes basal MEC function directly. Altogether, our data demonstrate, in different model systems, that adhesion to LM-521 leads to decreased progenitor and regenerative capability of basal MECs.

Adhesion to laminin α5 enhances luminal and suppresses basal gene expression

To dissect how basal cell functions are regulated by LM-521 adhesion, we performed RNA sequencing of HMEC-FL2 cells grown on LM-111, LM-521 or on uncoated plastic. Intriguingly, adhesion to LM-111 autologously produced by basal cells, induced expression changes only in eight genes [false discovery rate (FDR)<0.05] when compared to cells from uncoated plates. In contrast, LM-521 adhesion induced expression changes in 944 genes (Fig. 2A; Table S1), out of which 939 were unique to LM-521 adhesion (Fig. 2A). Interestingly, several ECM associated genes were differentially expressed (incluiding *LAMA1*, *LAMA3* and *LAMA4*, *COL14A1*, *COL13A1*, *ITGA5*, *ITGA10* and *MMP13*) (Fig. 2A) implying that LM-521 binding results in global alterations in ECM adhesion and remodeling. Unexpectedly, we also noted that several luminal associated genes were upregulated (including *KRT8*, *KRT18*, *KRT81* and *WNT5B*) and basal-associated genes downregulated (including *KRT5* and *TP63*) on LM-521 (Fig. 2A). Accordingly, gene set enrichment analysis (GSEA; Subramanian et al., 2005) revealed that LM-521 grown cells acquired a luminal signature (Huper and Marks, 2007), whereas basal signature genes were downregulated (Fig. 2B). Additionally, mammary stem cell signature genes (Lim et al., 2010) were downregulated in LM-521 grown cells (Fig. 2B). We verified these findings by quantitative (q)PCR of the luminal markers *KRT8* [encoding keratin 8 (K8)] and *SEMA3B*, and the basal markers *TP63* and *LAMA3* (Fig. 2C). Adhesion to LM-521 also enhanced *Krt8* gene expression in primary luminal MMECs, and whereas LM-521 adhesion was not sufficient to induce *Krt8* expression in primary basal MMECs, it resulted in significant decrease in basal markers *Krt14* and *Krt5* [encoding K14 and keratin 5 (K5), respectively; Fig. 2D]. Interestingly, we also observed an increase in the *Lama5* expression in primary basal cells grown on LM-521. Given that *Lama5* is predominantly expressed by the luminal cells (Englund et al., 2021),
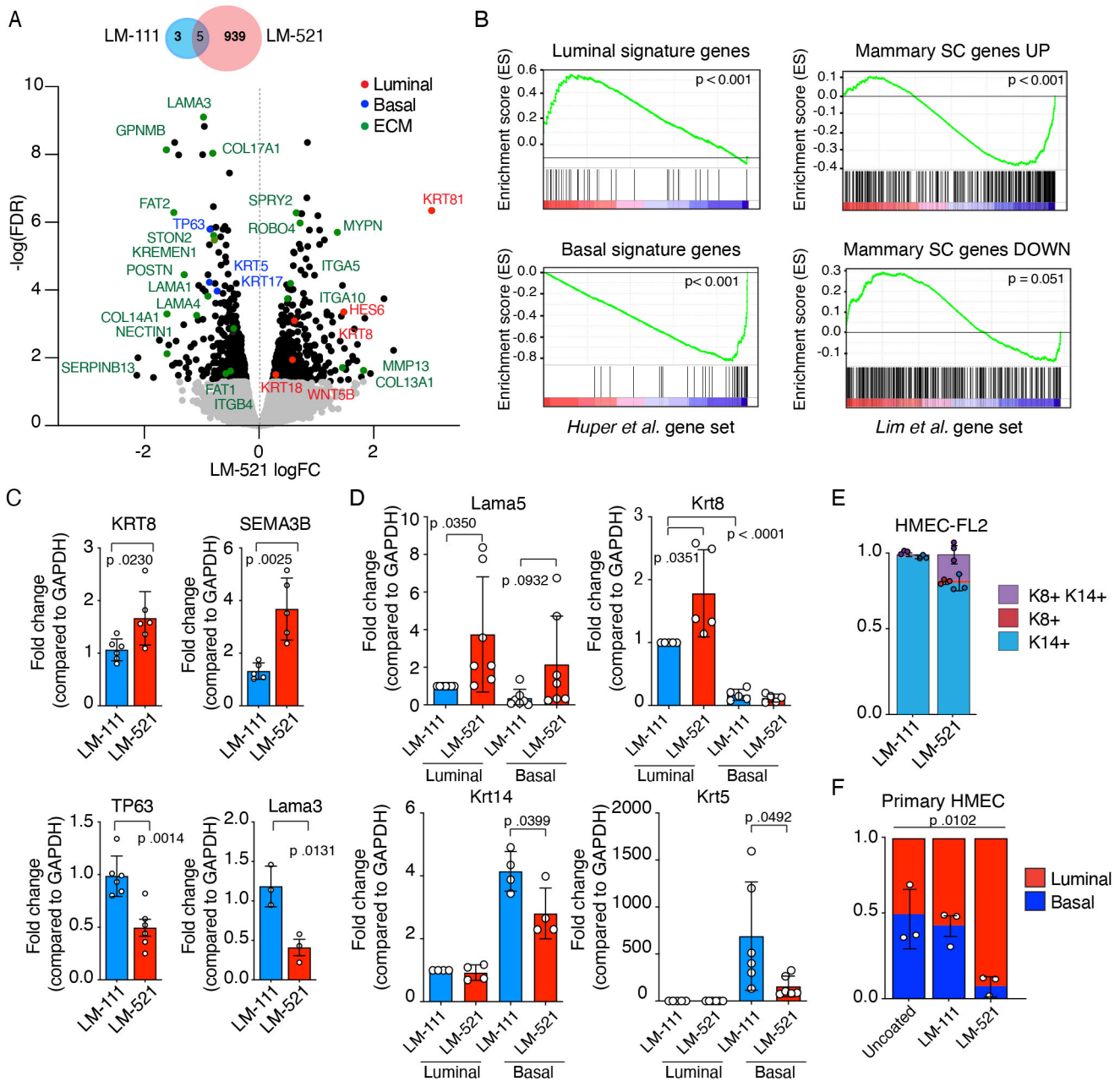
Fig. 2. LM-521 adhesion enforces luminal gene expression in luminal and basal MECs. (A) Top, Venn diagram showing differentially expressed genes (FDR<0.05) of HMEC-FL2 cells grown on LM-111 (blue circle) or LM-521 (red circle) for 48 h. Bottom, volcano plot showing differentially expressed genes in RNA sequencing of HMEC-FL2s grown for 48 h on LM-521 compared to uncoated control. The x-axis shows the log₂ of expression fold change and the y-axis log₂ of the FDR. Black dots represent genes with significantly increased or decreased expression (FDR<0.05). Selected genes related to luminal or basal differentiation or ECM are marked in red, blue or green, respectively. (B) GSEA plots showing correlation between the signature of HMECs grown on LM-521 and previously reported gene sets either downregulated or upregulated in basal MECs [gene set from Huper and Marks (2007)] or upregulated or downregulated in mammary stem cells [SC; gene set from Lim et al. (2010)]. (C) qPCR analysis of luminal (*KRT8* and *SEMA3B*) and basal (*TP63* and *LAMA3*) marker expression compared to *GAPDH* in HMEC-FL2s grown on LM-111 or LM-521 for 48 h. *KRT8* and *TP63*, n=6; *SEMAB*, n=5; *LAMA3*, n=4 independent experiments. (D) qPCR analysis of luminal (*Krt8* and *Lama5*) and basal (*Krt14* and *Krt5*) marker expression compared to *GAPDH* in basal (CD29hi/CD24+) and luminal (CD29low/CD24+) MECs grown on LM-111 or LM-521 for 48 h. All experiments are normalized to luminal MECs on LM-111. In all groups, *Krt8* n=5, *Krt14* n=4 independent experiments. (E) Quantification of frequencies of K14+, K8+ or double positive (K8+, K14+) HMEC-FL2 cells grown on LM-111 or LM-521 for 48 h. n=3 independent experiments. (F) Frequencies of luminal (EpCAM+) and basal (ITGA6+, CD10+) primary HMEC freshly isolated and grown on LM-111 or LM-521 or on uncoated plates. n=3 independent experiments. All data show mean±s.d. from independent experiments unless otherwise stated. An unpaired two-tailed Student's t-test was used to compare indicated groups.

these data suggest that adhesion to specific laminins might initiate a positive feed-forward loop in lineage specification. Thus, these results show that whereas LM-111 adhesion induces only minor alterations in basal MEC gene expression, adhesion to LM-521

enforces a luminal gene expression along with a decrease in basal marker expression. We additionally analyzed both trypsin detached and non-detached cells from same laminin pre-adhesion cultures by qPCR to exclude the possibility that the gene expression alterations

we observed result from selective harvesting of cells from pre-adhesion cultures. Both detached and non-detached cells showed similar differences in expression levels of *KRT8* and *TP63* between LM-111 and LM-521 (Fig. S3A), although expression levels were in general lower on detached cells. Taken together, despite the lower yield of cells from the LM-521 pre-adhesion (Fig. S2D), the similar level of initial cell adhesion after 4 h (Fig. S1E), proliferation, (Fig. S2F), death (Fig. S2H) and gene expression changes (Fig. S3A) jointly indicate that the laminin-specific effects on analyses downstream of pre-adhesion are not biased by selection of cells and represent qualitative changes induced during the pre-adhesion.

To analyze whether the differences observed in qPCR analyses were also seen at the protein level, we performed immunostaining of HMEC-FL2 cells grown on either LM-111 or LM-521 using K8 and K14 antibodies and quantified the frequency of cells positive for K8, K14 or both (K8+K14+). Whereas most of HMEC-FL2 stained negative for K8 on LM-111, we detected a clear increase in K8+ cells in LM-521 cultures and a corresponding increase in K8+K14+ cells compared to in cells grown on LM-111 (Fig. 2E). However, in both LM-111 and LM-521 cultures, the majority of cells expressed K14. These results imply that although LM-521 adhesion can enforce luminal gene expression and possibly a hybrid state between the cell types (Centonze et al., 2020), complete differentiation of basal cells into luminal cells requires additional factors. Intriguingly, however, these results suggest that laminin adhesion could differentially support growth of luminal and basal cells. To test this, we cultured unsorted primary HMECs on LM-111, LM-521 or on uncoated plastic. We observed that even by 24 h the frequency of luminal cells on LM-521 was clearly increased compared to that seen for uncoated or LM-111 grown HMECs (Fig. 2F; Fig. S3B). We furthermore analyzed the cultures by qPCR after 7 days (Fig. S3C) and detected higher expression of *KRT8* and *KRT19* levels and lower expression of *TP63* and smooth muscle actin (SMA; encoded by *ACTA2*) in LM-521 grown cells compared to LM-111 or uncoated cultures or to starting cultures at day 0 (Fig. S3C). To conclude, LM-521 adhesion also supports luminal MEC growth *in vitro*.

β1- and β4-integrin adhesion regulates downstream signaling of specific laminin matrices

To explore the signaling pathways regulating progenitor capabilities and luminal versus basal gene expression downstream of laminin adhesion, we examined the effects of specific laminin-binding integrins. We analyzed the protein expression of β1- and β4-integrins in HMEC-FL2 cells (Fig. S4A), which have been demonstrated to bind to both LM-111 and LM-521 (Ramovs et al., 2017; Yurchenco, 2011). Whereas β4-integrin protein levels remained unchanged, β1-integrin was reduced when cells were cultured on LM-521 (Fig. S4A). In accordance, we observed a decrease in the active form of β1-integrin in LM-521 grown cells (Fig. S4B). To investigate whether these β-integrins mediated the observed phenotypes, we downregulated each using RNA interference (RNAi; Fig. 3A, Fig. S4C) prior to laminin pre-adhesion. In LM-111 pre-adhesion cultured cells, β1-integrin downregulation led to a clear reduction in mammosphere formation, whereas downregulation of β4-integrin had no effect (Fig. 3B). In contrast, on LM-521, β1-integrin knockdown had no effects, but mammosphere formation was considerably increased by β4-integrin RNAi (Fig. 3B). Similarly, incubating cells in laminin pre-adhesion with the β1-integrin function-blocking antibody AIIB2 (Tomaselli et al., 1988) led to a decrease in mammosphere formation in LM-111 pre-adhesion cultures but not

in LM-521 (Fig. S4D). To investigate whether adhesion is affected in the siRNA-treated cells and could explain the differences in mammosphere formation, we performed IRM and analyzed the cell attachment area of AIIB2- or β4-integrin siRNA-treated cells and control cells. AIIB2 treatment completely abolished adhesion of cells to LM-111, but not to LM-521 (Fig. 3C). Reduced adhesion to LM-111, including clustering of cells, was observed even 48 h after initial seeding (Fig. 3C). Interestingly, however, downregulation of β4-integrin had no effect on cell adhesion kinetics on LM-111 or LM-521 (Fig. 3D), and cells appeared to be normally spread after 48 h. Thus, our data suggest that although loss of physical adhesion can play a part in decline of mammosphere formation in LM-111 cultured cells, LM-521 appears to affect mammosphere formation through other signaling mechanisms.

Next, we tested whether the expression of luminal and basal markers on LM-521 was altered by β-integrin knockdown. As expected, β1-integrin knockdown on LM-111 resulted in a decrease in *TP63* expression and no changes were observed in *KRT8* or *SEMA3B* expression (Fig. S4E). Also, no differences were seen with β1-integrin knockdown on LM-521 (Fig. S4E). However, *KRT8* expression was decreased and *TP63* expression increased in β4-integrin siRNA-transfected cells on LM-521 compared to control cells (Fig. 3E), showing that β4-integrin mediates the gene expression alterations in LM-521 adhered cells. In conclusion, our data corroborate previous studies showing that β1-integrin-mediated adhesion and LM-111 are required for maintenance of progenitor properties (Gudjonsson et al., 2002; Naylor et al., 2005; Taddei et al., 2008). Additionally, our data suggests that β4-integrin-mediated signaling from LM-521 might limit the progenitor capabilities through inducing luminal features.

PI3K activity induces progenitor activity irrespective of laminin adhesion

We next investigated signaling downstream of integrin adhesion and explored the PI3K signaling pathway, which integrates signals from growth factor receptors and cellular adhesion, for example, downstream of β1-integrin (Hemmings and Restuccia, 2012). Interestingly, in the mammary gland, mutated PI3K can induce multipotency in MECs (Koren et al., 2015). Therefore, we analyzed activation of the PI3K downstream effector Akt (herein referring to the Akt family) in HMEC-FL2 cells on laminin substrates by assessing the phosphorylation of threonine 308 (pT308 in Akt1 or equivalent residue on other Akt proteins) (Hemmings and Restuccia, 2012). Phosphorylation of Akt T308 was dramatically decreased in cells cultured on LM-521 (Fig. 4A), corresponding with reduced β1-integrin levels on LM-521. Next, we sought to determine whether the PI3K pathway mediates the effects of laminin adhesion on mammosphere formation and transduced HMEC-FL2 cells with a constitutively active mutant form of PI3K (H1047R; mutation is in the PIK3CA subunit of PI3K) (Fig. S5A,B). Strikingly, we observed increased mammosphere formation on LM-521 to a level comparable with LM-111 (Fig. 4B). Conversely, treatment of cells with the PI3K inhibitor LY294002 decreased mammosphere formation of LM-111 pre-adhesion cells considerably but resulted in only a negligible decrease on LM-521 (Fig. S5C,D). Interestingly, in qPCR analysis, we observed that *KRT8* and *TP63* expression was not modulated by laminin adhesion (Fig. 4C), suggesting mammosphere formation in PI3K (H1047R)-expressing cells is uncoupled from extracellular regulation. To conclude, we show that reactivation of PI3K pathway can overcome the LM-521 adhesion-induced decrease in basal MEC progenitor activity, and sustain basal
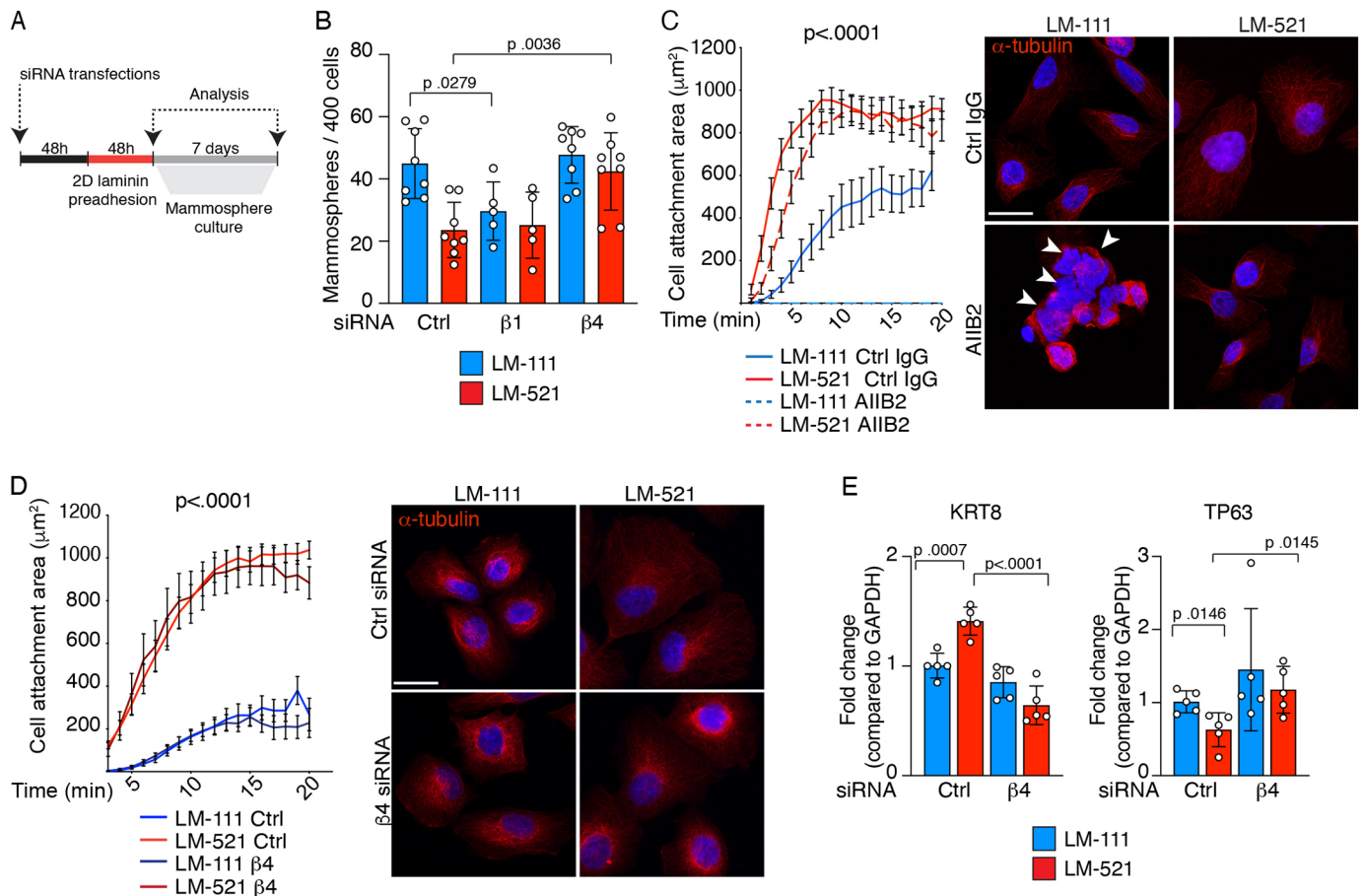
Fig. 3. LM-521 adhesion enforces luminal gene expression via β4-integrin. (A) Schematic of the experimental set-up with siRNA transfection and laminin pre-adhesion. (B) Mammosphere forming frequency of HMEC-FL2s treated with β1-integrin, β4-integrin or control siRNA and pre-adhered on indicated laminins as in A. *n*=8 independent experiments, except with β1-integrin *n*=5 independent experiments. (C) Quantification of cell attachment area of HMEC-FL2 treated with AIIB2 β1-integrin function blocking antibody or control IgG (left panel) using IRM at indicated time points after seeding on indicated laminins. Data show mean±s.e.m., *n*=3 independent experiments. Representative immunofluorescence images of HMEC-FL2s on LM-111 or LM-521 and stained with α-tubulin. Arrowheads point to cells not adhering to the laminin substrate. Scale bar: 20 μm. (D) Quantification of cell attachment area of HMEC-FL2 transfected with β4-integrin or control siRNA as in A using IRM at indicated time points after seeding on indicated laminins. Data show mean±s.e.m., *n*=3 independent experiments. Representative immunofluorescence images of HMEC-FL2s transfected with β4-integrin or control siRNA grown on LM-111 or LM-521 and stained with α-tubulin. Scale bar: 20 μm. (E) qPCR analysis of KRT8 and TP63 expression in HMEC-FL2 cells treated as in A. *n*=5 independent experiments. All data show mean±s.d. from independent experiments unless otherwise stated. Unpaired two-tailed Students *t*-test (B,E) or one-way ANOVA with Tukey's multiple comparison test (C,D) was used to compare indicated groups.

and luminal gene expression irrespective of laminin substrate adhesion.

Laminin adhesion regulates progenitor activity via p21

Given that expression of the PI3K (H1047R) mutant resulted in increased mammosphere formation of cells pre-adhered to LM-521, we investigated progenitor activity and self-renewal associated pathways downstream of PI3K. We explored the p53 pathway, which has been implicated in control of stemness and self-renewal in mammary progenitor cells (Chiche et al., 2013; Cicalese et al., 2009) and in regulation of mammary gland functionality downstream of integrin-α3 and -α6 adhesion (Romagnoli et al., 2020). Also, p53 effector cyclin dependent kinase (CDKI) inhibitor p21 (encoded by the *CDKN1A* gene) has been suggested to regulate basal stem cell quiescence in the mammary epithelium (Cai et al., 2017) and to be regulated upstream by β1- and β4-integrin (Clarke et al., 1995; Li et al., 2005).

Intriguingly, our RNA sequencing showed that *CDKN1A* expression was upregulated in HMEC-FL2 cells pre-adhered to

LM-521 (Table S1; Fig. 4D), and we did not observe stabilization of p53 in LM-521 grown cells (Fig. S5E). To establish whether the p53–p21 pathway regulates mammosphere formation downstream of laminin adhesion, we treated pre-adhered cells with 1 μM Nutlin-3, a small molecule compound inducing p53 re-activation (Vassilev et al., 2004). Nutlin-3 treatment led to an increase in p21 immunostaining without widespread cell death (Fig. S5F,G), and decreased mammosphere formation of LM-111 pre-adhered cells, whereas cells on LM-521 were unaffected (Fig. 4E). Also, mammosphere formation driven by the PI3K (H1047R) mutant was diminished with Nutlin-3 treatment (Fig. 4F) although no decrease in Akt T308 phosphorylation was observed (Fig. S5G). Next, we investigated whether the p53–p21 pathway is responsible for regulation of mammosphere formation downstream of β4-integrin. Thus, we treated cells with β4-integrin knockdown with Nutlin-3 during laminin pre-adhesion. Interestingly, p53 reactivation led to a decrease in mammosphere formation in LM-111 grown control cells except in the β4-integrin downregulated cells (Fig. 4G). This implies that β4-integrin downregulation renders
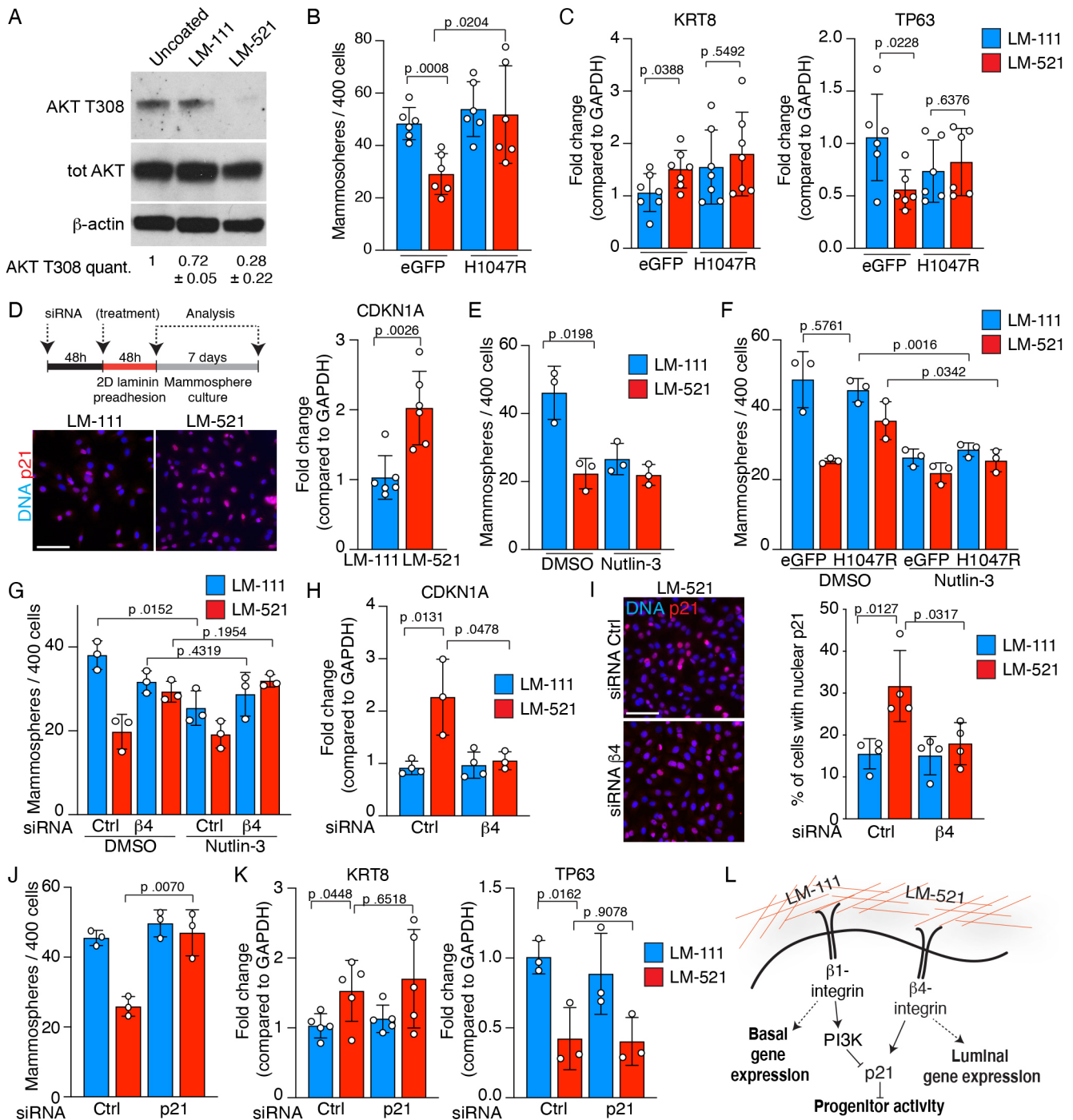
Fig. 4. See next page for legend.

cells at least partly insensitive to p53 reactivation, for instance due to altered p53 signaling or decreased p21 expression levels in β4-integrin deficient cells. Indeed, siRNA knockdown of β4-integrin inhibited the p21 upregulation in LM-521 pre-adhered cells (Fig. 4H,I), demonstrating a link between β4-integrin-mediated adhesion and p21. Finally, we addressed whether p21 loss led to increased progenitor activity in basal MECs, and downregulated p21 using siRNA (Fig. S4I). Although there was no difference in mammosphere formation in cells pre-adhered to LM-111, p21 deficiency led to a clear increase in mammosphere formation following LM-521 treatment (Fig. 4J).

To investigate whether p21 regulates luminal and basal gene expression downstream of laminin adhesion, we performed qPCR for *KRT8* and *TP63* (Fig. 4K). Surprisingly, we did not observe differences in expression of either gene in control or p21 siRNA-treated samples in LM-111 or LM-521 adhered cells. Taken together, based on our data, we propose a working model, where β1- and β4-integrin-mediated adhesion to laminin controls basal and luminal gene expression and p21 levels to define basal MEC progenitor activity (Fig. 4L). Signaling via LM-111 through β1-integrin and activated PI3K increases basal MEC progenitor activity through negative regulation of p21, whereas signaling via LM-521

Fig. 4. β1-integrin–PI3K and β4-integrin signaling regulate progenitor activity via p21. (A) Western blot of AKT T308 phosphorylation and total AKT levels of HMEC-FL2 cells grown on different laminins for 48 h. Below shown the quantification of pAKT band intensity (±s.d. from three independent experiments) compared to total (tot) AKT and normalized to actin. (B) Mammosphere forming frequency of HMEC-FL2s expressing PI3K (H1047R) or eGFP and pre-adhered on indicated laminins for 48 h. n=5 independent experiments. (C) qPCR analysis of *KRT8* and *TP63* expression in HMEC-FL2 PI3K (H1047R)- or eGFP-expressing cells pre-adhered on the indicated laminins for 48 h. n=5 independent experiments. (D) Schematic of the experimental set-up with siRNA transfection, additional treatment and laminin pre-adhesion. Representative images from three experiments HMEC-FL2 cells grown on indicated laminins and immunostained with p21 antibody and Hoechst to visualize DNA and qPCR analysis of *CDKN1A* expression levels compared to *GAPDH* of the same cells. n=6 independent experiments. Scale bar: 50 μm. (E) Mammosphere forming frequency of HMEC-FL2s pre-adhered on indicated laminins and concurrently treated with 1 mM Nutlin-3 or DMSO as control. n=3 independent experiments. (F) Mammosphere forming frequency of HMEC-FL2s expressing PI3K (H1047R) or eGFP and treated with 1 mM Nutlin-3 or DMSO as control. n=3 independent experiments. (G) Mammosphere forming frequency of HMEC-FL2s transfected with β4-integrin or control siRNA, pre-adhered on indicated laminins and treated with 1 mM Nutlin-3 or DMSO as control. n=3 independent experiments. (H) qPCR analysis of *CDKN1A* expression in HMEC-FL2 transfected with β4-integrin or control siRNA and pre-adhered on indicated laminins for 48 h. n=4 independent experiments for LM-111 and n=3 for LM-521. (I) Representative images from three experiments of siRNA-transfected HMEC-FL2 cells grown on indicated laminins and immunostained with p21 antibody and Hoechst to visualize DNA. Scale bar: 50 μm. Right graphs shows quantification of nuclear p21 frequency of siRNA-transfected HMEC-FL2 cells. n=4 independent experiments. (J) Mammosphere forming frequency of HMEC-FL2s transfected with *CDKN1A* or control siRNA and pre-adhered on indicated laminins. n=3 independent experiments. (K) qPCR analysis of *KRT8* and *TP63* expression in HMEC-FL2 cells transfected with *CDKN1A* or control siRNA and pre-adhered on indicated laminins. n=4 (*KRT8*) or n=3 (*TP63*) independent experiments. (L) Working model suggesting how laminin adhesion regulates gene expression and progenitor activity via p21. All data show mean±s.d. from independent experiments unless otherwise stated. An unpaired two-tailed Student's t-test was used to compare indicated groups.

by β4-integrin leads to an increase in p21 levels and activity and decrease in the basal MEC progenitor activity.

Laminin adhesion regulates basal MEC plasticity

Basal MECs exhibit remarkable plasticity under specific physiological conditions and in the mammary reconstitution assay to build an intact tissue (Centonze et al., 2020; Shackleton et al., 2006; Stingl et al., 2006). Given that LM-521 pre-adhesion resulted in a lower reconstitution potential, we explored whether laminin adhesion regulates MEC plasticity. To do this, we modified a 3D Matrigel culture method, where single basal MECs are induced to generate branching organoids that consist of both basal and luminal MECs (Jamieson et al., 2017). We investigated whether addition of LM-111 or LM-521 into 3D Matrigel matrix affects formation of branching organoids (Fig. 5A; Fig. S6A) and therefore plasticity of the basal cells. Interestingly, we observed that organoids in LM-521 mixed cultures (M+521) formed branches with significantly lower frequency than organoids in LM-111 mixed culture (M+111) (Fig. 5B,C). The number and size of spheroids starting at day 3 was similar (Fig. S6B), indicating that the presence of LM-521 hampers the ability of basal MECs to generate branching organoids without affecting initial growth. To determine whether LM-521 adhesion directly affects the capability of basal cells to generate cells of luminal lineage, we immunostained cells grown in M+111 or M+521 for 3 days with K8 and K14 antibodies. We examined organoids with two cells to observe cells after the first cell division in culture. Whereas organoids

forming from luminal cells faithfully expressed only K8 staining, and majority of basal cells only K14, surprisingly a portion of the basal two-cell organoids were positive for the luminal marker K8 (Fig. 5D). Importantly, the frequency of K8 positivity of basal organoids was higher on M+521 than on M+111 (Fig. 5D,E). In larger organoids with more than five cells, a clear majority had K8-positive cells (Fig. 5E), suggesting adhesion to LM-521 induces differentiation of cells towards the luminal lineage. Moreover, in our culture system, the frequency of luminal cells forming branching organoids was <10% (Fig. S6C) compared to the 40–60% of basal cells that formed organoids. Therefore, and as the organoid branching requires balanced generation of both luminal and basal cells (Jamieson et al., 2017), these data suggest that the enforcing of luminal gene expression by LM-521 disturbs this balance. Thus, we conclude that LM-521 does not directly inhibit plasticity, but instead overdrives basal cells into the non-plastic luminal identity.

To investigate whether β4-integrin signaling also regulates branching structure formation downstream of LM-521, we transduced primary basal MECs with β4-integrin (*Itgb4*) or control (scrambled; SCRA) CRISPR guides (Fig. 5F; Fig. S6D). Basal MECs with *Itgb4* knockdown exhibited equal amounts of branching organoids at 14 days when cultured in M+111 compared to control MECs. Interestingly, branching occurred in M+521 cultures at similar levels to in M+111 cultures, implying that *Itgb4* targeting can rescue the LM-521-induced decrease in branching morphogenesis (Fig. 5G, H). Hence, these and our above results demonstrate that β4-integrin mediates signaling from LM-521.

Laminin α5 modulates basal MEC plasticity *in vivo*

Next, we investigated whether reduction in laminin α5 *in vivo* affects primary basal MEC characteristics. In the mammary gland, luminal cells are the major source of laminin α5 (Englund et al., 2021), and thus we treated post-pubertal 8 weeks old *Lama5* fl/fl; K8-CreERT2 (Englund et al., 2021) and control mice with tamoxifen to delete Lama5 from the luminal epithelial cells. The adjacent basal MECs were isolated 6 weeks later at 14 weeks of age (Fig. 6A). At this timepoint, we observed downregulation of *Lama5* mRNA (Fig. S6E), whereas combined frequency of EpCAM+ cells remained unchanged (Fig. S6F,G). Strikingly, basal MECs from *Lama5* fl/fl mice formed branching organoids at a higher frequency in both M+111 and M+521 cultures (Fig. 6B), yet the number of organoids initiated by day 3 and organoid size at day 7 were not significantly different between the groups (Fig. S6H). In agreement with our previous results, presence of LM-521 in the cultures reduced the number of branching organoids compared to LM-111 in both cases (Fig. 6C). Moreover, the early day 3 organoids from the *Lama5*-deficient glands were K8 positive at a lower frequency than organoids from control glands (Fig. 6D), indicating that the reduction of *Lama5 in vivo* had reduced the adoption of luminal traits by basal cells, and thereby increased their ability to generate branching organoids that require balanced production of both cell types. In line with this notion, basal MECs from *Lama5*-deficient glands expressed elevated levels of basal marker *Krt14* and *Ezh2* (Fig. 6E), a histone methyltransferase previously linked with activation of mammary progenitor state and stem cell maintenance (Margueron and Reinberg, 2011; Pal et al., 2017), and a modest, yet statistically not significant, increase in basal marker *Krt5* (Fig. 6E). Jointly these results imply that, although basal cells originating from *Lama5*-deficient mammary tissue do not exhibit increased progenitor activity, they might be primed for multipotency.

Finally, we asked whether the p21 pathway regulates basal MEC function. In accordance with our HMEC data, basal MEC organoids
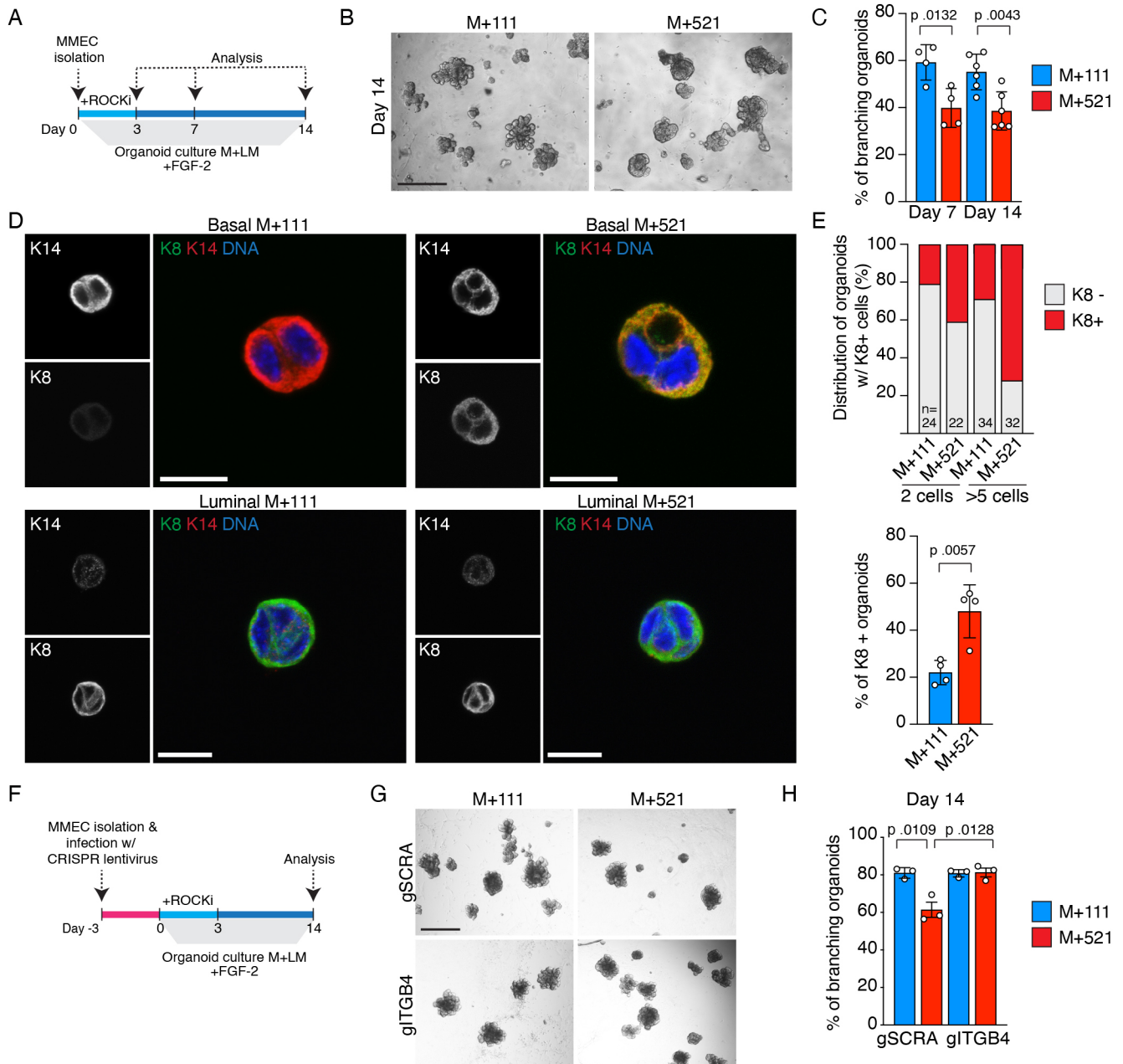
Fig. 5. Laminin α5 adhesion regulates basal MEC plasticity through β4-integrin. (A) Schematic of the organoid culture set-up, where FACS sorted primary MECs are cultured in Matrigel (M) culture supplemented with 20 mg/ml LM. (B) Representative phase-contrast images from four experiments of basal MECs cultured as in A either with LM-111 (M+111) or LM-521 (M+521) for 14 days. Scale bar: 200 µm. (C) Frequency of branching organoid formation of basal MECs grown either in M+111 or M+521 culture for 7 or 14 days. $n=4$ independent experiments. (D) Representative immunofluorescence images from four experiments of MECs cultured in M+LM culture for 3 days and immunostained to detect K8 or K14. Scale bars: 10 µm. (E) Upper graph shows the proportions of K8 positivity in day 3 M+111 and M+521 cultured organoids with 2 or >5 cells. Shown is pooled data from 4 animals, number of organoids analyzed is shown within the graph. Lower graph shows the average frequency of organoids with K8+ cells in M+111 and M+521 cultures. $n=4$ independent experiments. (F) Schematic of the organoid culture set-up, where freshly isolated and FACS sorted basal MECs are infected using lentiviruses carrying either SCRA or ITGB4 CRISPR guide and cultured in M+LM culture. (G) Representative phase-contrast images from three experiments of basal MECs treated as in A and cultured either with LM-111 (M+111) or LM-521 (M+521) for 14 days. Scale bar: 200 µm. (H) Frequency of branching organoid formation of basal MECs expressing gSCRA or gITGB4 and grown either in M+111 or M+521 culture for 14 days. $n=3$ independent experiments. All data show mean±s.d. from independent experiments unless otherwise stated. An unpaired two-tailed Student's t-test was used to compare indicated groups.

exhibited nuclear p21 immunostaining with significantly higher frequency when grown in M+521 compared to in M+111 (Fig. 6F,G). Intriguingly, the p21 levels in all *Lama5* fl/fl organoids were comparable to those in control M+111 cultures, suggesting that basal *Lama5* fl/fl cells are refractory to laminin signals, likely due to their primed state. However, the low p21 frequencies

correlated clearly with K8 frequencies (Fig. 6G). We tested also whether activation of the p53–p21 pathway inhibits formation of branching structures and treated organoids in M+111 culture with Nutlin-3. Although the initial number of spheroids was not decreased (Fig. S6I), the number of branching organoids was diminished upon Nutlin-3 treatment (Fig. S6J) suggesting that the
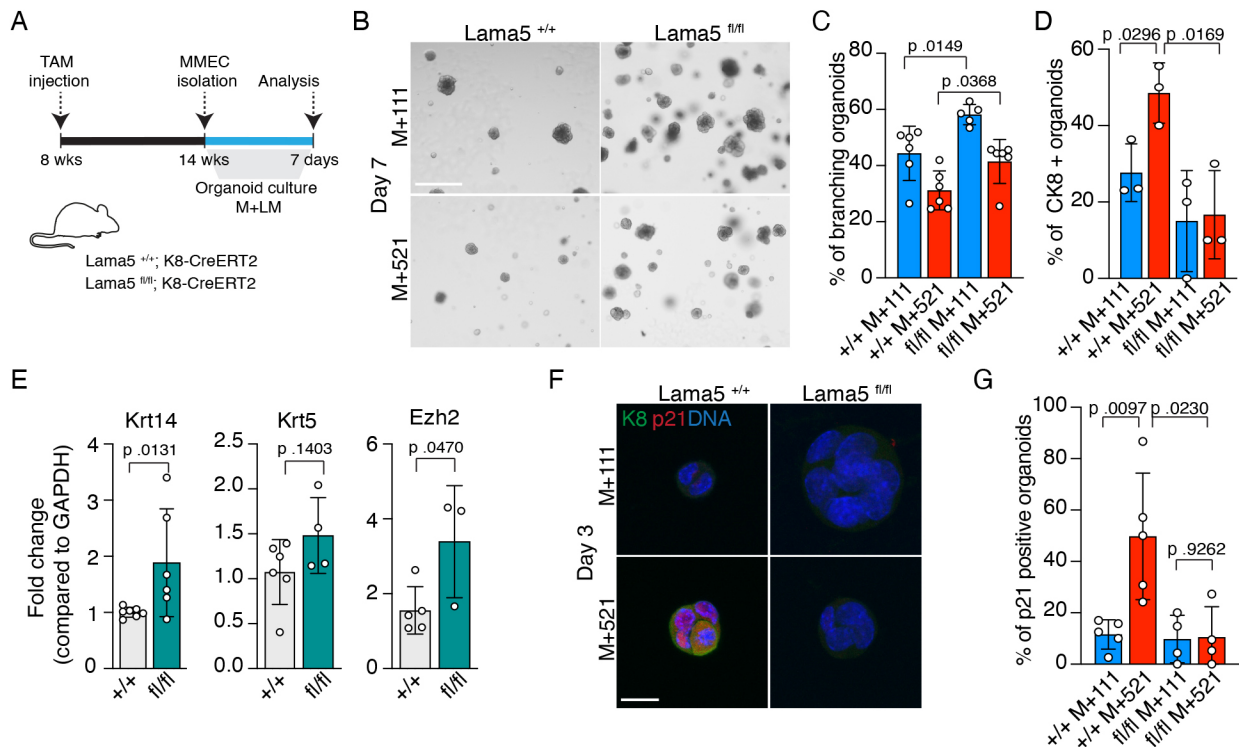
Fig. 6. Reduction of laminin α5 *in vivo* alters basal MEC plasticity. (A) Schematic of the experimental set-up, where *Lama5*fl/fl;K8-CreERT2 and control mice are treated with tamoxifen at 8 weeks and MMECs are isolated and FACS sorted at 14 weeks. (B) Representative phase-contrast images from three experiments of organoids from *Lama5*fl/fl;K8-CreERT2 and control mice cultured in M+111 and M+521 for 7 days. Scale bar: 200 µm. (C) Frequency of branching organoid formation of basal *Lama5*fl/fl;K8-CreERT2 and control MECs cultured in M+111 and M+521 for 3 days. *Lama5*+/+ *n*=6 and *Lama5*fl/fl M+111 *n*=5 independent experiments. (D) The frequency of K8+ cells in *Lama5*fl/fl;K8-CreERT2 and control organoids in day 3 M+111 and M+521 cultures. *n*=3 independent experiments. (E) qPCR analysis of *Krt14*, *Krt5* and *Ezh2* expression in freshly isolated basal *Lama5*fl/fl;K8-CreERT2 and control MECs. Krt14 *n*=6/6 (+/+ / fl/fl), *Krt5 n*=6/4 and *Ezh2 n*=5/3 independent experiments. (F) Representative immunofluorescence images from three experiments of *Lama5*fl/fl;K8-CreERT2 and control organoids immunostained to detect K8 and p21. Scale bar: 10 µm. (G) The frequency of *Lama5*fl/fl;K8-CreERT2 and control organoids with p21+ cells in M+111 and M+521 cultures. *Lama5*+/+ *n*=5 and *Lama5*fl/fl *n*=4 independent experiments. All data show mean±s.d. from independent experiments unless otherwise stated. An unpaired two-tailed Student's *t*-test was used to compare indicated groups.

p53–p21 pathway is critical for their formation and likely an essential regulator of basal MEC characteristics. Furthermore, our data show that basal cells can be primed for multipotency *in vivo*. However, to preserve tissue integrity, such basal cell traits are only observed in response to permissive signals or environment.

DISCUSSION

Growth and differentiation of the mammary epithelium needs to be tightly regulated to generate appropriate amounts of differentiated cell types to ensure tissue functionality. Although the role of ECM and more specifically laminins has been appreciated in growth and differentiation of MECs (Gudjonsson et al., 2002; Inman et al., 2015), how specific laminin components affect mammary epithelial growth or lineage identity has been unclear. Here, we show that laminin matrix adhesion is a central regulator of gene expression, and basal cell characteristics and identity in both human and mouse MECs. We have previously shown that laminin α5, produced for the major part by luminal epithelial cells (Englund et al., 2021), is critical for the differentiation of luminal MECs. It is especially important for the HR+ luminal MECs, which orchestrate the mammary gland growth in response to systemic hormones (Feng et al., 2007). In the absence of laminin α5, HR+ cells fail to support adjacent basal cells through secretion of Wnt4, which leads to restrained growth of the entire epithelium. Here, we demonstrate that adhesion of basal MECs to laminin α5-containing LM-521 matrix, decreases the basal MEC function including the capability to form mammospheres and to

reconstitute mammary gland. Importantly, we show that adhesion to LM-521 matrix activates a luminal gene expression program and promotes features of luminal identity in the basal cells.

We show that LM-521 matrix adhesion restricts basal gene expression via suppression of the β1-integrin–PI3K signaling pathway and enforces luminal gene expression and p21 activation via β4-integrin (Fig. 4L, working model). These results are in line with previous work showing that β1-integrin signaling is essential especially for basal MEC function and progenitor activity (Li et al., 2005; Taddei et al., 2008). Moreover, we show that loss of β1-integrin leads to loss of cell adhesion specifically to LM-111, which can in part underlie the importance of β1-integrin in the mammary epithelium as well as in morphogenesis of other tissues (Wang et al., 2021). In contrast, the role of β4-integrin in the mammary gland physiology has remained more ambiguous. Although β4-integrin is expressed in both luminal and basal mammary epithelial cells, its depletion does not appear to severely compromise mammary gland growth *in vivo* (Klinowska et al., 2001; Li et al., 2015; Yang et al., 2009). This could be explained in the light of our current results, as we show that loss of β4-integrin does not compromise cell adhesion, but β4-integrin regulates p21 activity and luminal gene expression downstream of LM-521 adhesion. Therefore, loss of β4-integrin would not be expected to interfere with epithelial growth. Interestingly, previous studies have linked β4-integrin into cell cycle progression via amplifying growth factor signaling especially in cancer cells (Guo et al., 2006), and into growth

inhibition via p21 and p27 (Clarke et al., 1995; Murgia et al., 1998). p21 has been established in regulation of stem and progenitor cell proliferation in multiple tissues (Cai et al., 2017; Cheng et al., 2000; Marqués-Torrejón et al., 2013) and in the mammary gland it has been implicated in basal progenitor cell quiescence downstream of Bcl-11b to preserve the long-term regenerative capacity of the epithelium (Cai et al., 2017). Furthermore, p21 has been shown to be upregulated downstream of p53 in double α3/α6-integrin knockout in basal MECs (Romagnoli et al., 2019). Interestingly, in our assays, silencing of p21 did not affect the upregulation of luminal gene expression downstream of LM-521 adhesion, suggesting that epithelial gene expression could be regulated independently of progenitor activity. In homeostatic tissues, regulation of progenitor activity and self-renewal separately from differentiation cues can present a mechanism to quickly restore multicellular tissue architecture and function, for instance in case of an injury, as has been shown to occur in epidermis during wound healing (Ge et al., 2017).

Our results indicate that adhesion to a laminin α5-rich matrix suppresses basal identity, including plasticity. This can be seen by the lowered capability of LM-521-adhered basal MECs to generate organoids consisting of both basal and luminal lineage cells, likely due to the basal cells quickly adopting luminal identity and preventing formation of bi-lineage organoids. Interestingly, basal cells from *Lama5*-deficient mammary epithelium form bi-lineage organoids with increased frequency, suggesting they are primed for multipotency in their *in vivo* environment. These results are in line with a previous study showing that luminal mammary epithelial cells are critical in restricting the basal cell plasticity during homeostasis *in vivo* and *in vitro* by secreting tumor necrosis factor (TNF) (Centonze et al., 2020). It is possible that luminal cells regulate basal cell multipotency with soluble factors and with more stable factors, such as laminins incorporated into the BM, to ensure both rapid remodeling during pregnancy and structural stability of the multicellular tissue in the long term. To conclude, our study shows matrix adhesion acts as a key upstream regulator of tissue level plasticity and cell identity to ensure functionality of the mammary epithelium beyond its role as platform for attachment.

MATERIALS AND METHODS
Animal studies
All animal studies were approved by the National Animal Ethics Committee of Finland (ELLA) and conducted in the Laboratory animal center (LAC) of the University of Helsinki under institutional guidelines. *Lama5 flox* and *K8-CreERT2* mouse lines have been previously described, and genotyping was performed using previously described primers (Nguyen et al., 2005; Van Keymeulen et al., 2011). For K8-CreERT2 induction, a single dose of 5 mg tamoxifen in corn oil (both from Sigma) was injected intraperitoneally in 8-week-old mice.

For the fat pad reconstitution assay, mammary epithelial cells were isolated from 10–16-week-old wild-type C57BL6/RccHsd donor mice as described below. 3-week-old female C57BL6/RccHsd mice were anesthetized using 2–2.5% isoflurane (Baxter) and the anterior part of the #4 mammary gland, lymph node and bridge to the #5 gland were surgically removed. To the remaining fat pad, 10^5 cells/gland were injected in 10 µl volume using a Hamilton syringe. The wound was sutured using wound clips (Autoclip Physicians kit, Becton Dickinson), which were removed 1 week after the operation. The transplanted mice were euthanized 8 weeks after transplantation.

Cell culture, treatments and transfections
The HMEC FL2 cell line (a gift from Dr Christine Chaffer, The Kinghorn Cancer Centre, Garvan Institute of Medical Research, Sydney, Australia), was cultured as previously described (Chaffer et al., 2011) in mammary epithelial basal medium (MEGM; Lonza) and routinely tested for mycoplasma contamination. For laminin pre-treatment assays, glass coverslips or 12-well plates (Nunc) were coated with 50 µg/ml of laminin-111 or -521 (BioLamina) at +4°C overnight before seeding cells. In indicated experiments, cells were treated with the following reagents during laminin pre-treatment assays: AIIB2 antibody (20 µg/ml, Millipore), control IgG from same species (20 µg/ml, Biolegend), LY-294002 (10 µM, Sigma) or Nutlin-3 (1 µM, Enzo Lifesciences). For mammosphere culture, cells were cultured in 1% methylcellullose (Sigma) in MEGM on 96-well ultra-low attachment plates (Corning) for 7 days at the indicated densities. For secondary mammosphere culture, primary mammospheres were collected, dissociated with 0.05% Trypsin-EDTA (DIFCO, J.T. Baker), and counted at day 7 and replated in methylcellulose for an additional 7 days. The process was repeated for tertiary mammosphere culture. For siRNA, HMECs were transfected on 6-well plates with 500 µg of esiRNA pool (Sigma) targeting either human β1-integrin (EHU065071), β4-integrin (EHU059511) or *CDKN1A* (EHU003861) (or siLuc as negative control; EHUFLUC) for 4 h using Dharmafect transfection reagent (Dharmacon) in antibiotic-free MEGM according to the manufacturer's instructions. Thereafter the medium was changed to normal MEGM and cells were incubated 48 h before trypsinization and plating in experiments.

Primary MMEC isolation
Primary mouse mammary epithelial cells (MMECs) were isolated from 10–16-week-old virgin female mice unless otherwise stated. Shortly after, mammary glands #3–5 were dissected. The lymph node in #4 glands was removed and the glands were finely chopped. Tissue was incubated with 0.01 mg collagenase A (Sigma) per 1 g of tissue in advanced DMEM/F12 growth medium (Life Technologies) containing 2.5% FCS, 5 µg/ml insulin, 50 µg/ml gentamicin and 2 mM glutamine with gentle shaking (120 rpm in an environmental shaker) at 37°C for 2–2.5 h. The resulting cell suspension was then first centrifuged at 400 *g* for 10 min and consecutively pulse centrifuged 3–5 times at 400 *g* to get a preparation free of cells other than MMEC organoids. Next organoids were trypsinized with 0.05% Trypsin-EDTA (DIFCO, J.T. Baker) for 5–10 min and drained through 70 µm cell strainer to obtain single cells and centrifuged at 300 *g* for 5 min. The cell pellet was resuspended in MMEC growth medium [advanced DMEM/F12 containing 5 µg/ml insulin, 1 µg/ml hydrocortisone, 10 ng/ml mouse EGF, 2 mM glutamine, 50 µg/ml gentamycin and penicillin and streptomycin (all from Sigma) supplemented with 10% FCS (Gibco)] for further experiments or cells were subjected to FACS sorting for separating basal and luminal MMECs (see below).

FACS sorting of primary MMECs
Single-cell suspensions of isolated primary MMECs were resuspended in 0.2% BSA in Dulbecco's PBS and the cells were incubated with either of the following sets of primary antibodies: CD31–PE, CD45–PE, Ter119–PE, CD24–Pacific Blue (from Becton Dickinson) and CD29–FITC (from Sigma), or CD29–FITC (Miltenyi Biotec, 130-102-975), CD326 (Ep-CAM) BV786 (BD; 740958), CD45 PerCP–Cy5.5 (Tonbo Biosciences; 65-0452-U100), CD31 PerCP–Cy5.5 (BD; 562861) and Ter-119 PerCP-Cy5.5 (BD; 560512). All antibodies were used at 1:500 and incubated on ice for 30 min. Cells were washed with PBS and re-suspended in 0.2% BSA in Dulbecco's PBS with 1 µg/ml 7-AAD (Life Technologies, Thermo Fisher Scientific) to exclude dead cells. Sorting was performed with a BD FACSAria Fusion Flow Cytometer (lasesr 405 nm, 488 nm, 561 nm ans 633 nm) (Beckton Dickinson). FlowJo V10 software was used for post-analysis of sorted cells.

2D and 3D cell culture of primary MMECs
For laminin pre-treatment assays, cell culture plates or coverslips were coated similarly to was done for HMEC-FL2 with recombinant laminins. For mammosphere culture, cells were cultured in 1% methylcellullose (Sigma) in DMEM/F12 growth medium on 96-well ultra-low attachment plates (Corning) for 14 days in indicated densities. 3D organotypic culture was performed in growth factor-reduced basement membrane from Engelbreth–Holm–Swarm (EHS) mouse sarcoma (Matrigel™, Becton Dickinson), which was prepared according to manufacturer's instructions. Isolated and FACS sorted primary MMECs were suspended with liquid Matrigel supplemented with either PBS, LM-111 or LM-521 (20 µg/ml)

and plated onto 8-chamberslides in Matrigel mixture drops, with ~2000 cells/drop. Organoids were grown in MMECs growth medium (see 'Primary MMEC isolation' section) supplemented with 500 ng/ml R-spondin (R&D Systems), 100 ng/ml noggin (PeproTech), 2.5 nM FGF2 (Novus Biologicals) and 10 µM Y27632, which was added for the first 2-3 days of culture. After 7 days media was finally switched to Advanced DMEM/F12 media supplemented with 2.5 nM FGF2 and 1X ITS (Sigma-Aldrich), which was refreshed every 3-4 days.

Reduction mammoplasty and human primary cell culture

Primary human mammary epithelial cells (HMECs) were isolated from breast tissue obtained from reduction mammoplasty operations of healthy volunteers upon written informed consent (ethical approval ETKM 23/ 2018 from the Ethical committee of Hospital District of Southwest Finland). All clinical investigations have been conducted according to the principles expressed in the Declaration of Helsinki. The tissue was transferred in transport medium [5% fetal bovine serum (FBS; Sigma) and 10 mM HEPES pH 7.5 (Sigma) in DMEM/F12 GlutaMAX (Gibco)]. After the removal of extra fat, the tissue was dissected into pieces of ~1 mm^3 and enzymatically digested in an environmental shaker (120 rpm) in dissociation medium [penicillin-streptomycin 1:100, 5% FBS, filter-sterilized collagenase (300 U/ml, type XI, Sigma) and hyaluronidase (100 U/ml, type I-S, Sigma) in MEGM (Promocell)] at 37°C overnight. The dissociated glandular tissue was centrifuged for 5 min at 600 g. Cell pellets were resuspended in 10 ml of transport medium with 10 µg/ml DNase I from bovine pancreas (Sigma), shaken occasionally for 1 min to digest DNA, and pelleted and resuspended in 10 ml of transport medium. The tissue was pulse centrifuged twice for 1 min and twice for 30 s at 80 g, whereafter the pellet was collected.

To yield single cells, the epithelial structures were trypsinized in 0.25% trypsin-EDTA (Gibco) on a 6-well low-adhesion cell culture plate (Sigma) at 37°C. Cells were pelleted for 5 min at 600 g and treated with dispase II (5 mg/ ml, Roche) diluted 1:1 in MEGM with DNase (10 µg/ml) and suspended with a pipette for 1 min. Cells were pelleted again, resuspended in MEGM, and filtered through a 40 µm cell strainer (Thermo Fisher Scientific). Primary HMEC organoids were cultured as previously described (Linnemann et al., 2017). Briefly, single primary epithelial cells (2500 cells/well) were seeded within a collagen matrix (1.3 mg/ml, PureCol® EZ Gel; Advanced Biomatrix) into a low adhesion 24-well plate containing no additional components or LM-521 (5 µg/ml, rhLaminin-521, Thermo Fisher Scientific) and allowed to polymerize at 37°C for 1 h. Next, culture medium [MEGM with 5 µM Y-27632 (Santa Cruz Biotechnology) and 0.8% FBS] was added on top and gels detached from wells allowing them to float. Y-27632 was removed from the medium after 5 days in culture. Organoids were cultured for 14 days, after which they were fixed (4% PFA) and counted. Coherent and 3D structures without distinct single cells were counted as organoids.

Immunofluorescence staining and imaging

2D coverslip-grown HMEC-FL2 and MMEC samples were fixed with 4% PFA at room temperature (RT) for 10 min. After fixation, cells were washed with PBS and permeabilized with 0.1% Triton-X (Sigma) in PBS for 5 min. Next, samples were washed twice with PBS and non-specific binding sites were blocked with 10% FBS in PBS for 30 min, and thereafter incubated with primary antibodies (α-tubulin, Cell Signaling 3873, 1:500; cleaved caspase-3, Cell Signaling 9661, 1:500; K8, Developmental Studies Hybridoma Bank TROMA-1, 1:300; K14, Biolegend 905301, 1:300; β1-integrin 12G10 Abcam ab30394, 1:300; p21, Cell Signaling Technologies 2947, 1:300) diluted in blocking solution (10% FBS in PBS) at RT for 1 h. Following incubation, samples were washed three times with PBS and then incubated for 30 min in RT with appropriate Alexa Fluor (Life Technologies) secondary antibodies (either Alexa Fluor 488 or Alexa Fluor 545). Finally, samples were washed three times with PBS followed by counterstaining of nuclei with Hoechst 33342 (Sigma).

Primary HMECs were fixed with 4% PFA at RT for 10 min. Cells were once flushed and once washed with PBS for 5 min and thereafter permeabilized with 0.1% Triton X-100 in PBS in RT for 10 min. Next, cells were incubated in 10% horse serum in 0.1% Tween-20 in 1× Tris-buffered saline (TBS; 0.1% TBST) blocking buffer in RT for 1 h. Antibody mixture was prepared in blocking buffer with antibodies against CD10 (1:10,

APC-conjugated, Invitrogen, MA1-19733), EpCAM (1:50, Alexa555-conjugated, Cell Signaling Technology, 5488S), and human integrin α6 (ITGA6) (1:50, Alexa488-conjugated, R&S Systems, FAB1350V-100U). Cells were incubated in staining solution on a shaker in RT for 1 h and kept in PBS at +4°C until imaged. Images were taken with a 3i spinning disk confocal microscope (Intelligent Imaging Innovations Inc., Denver, Colorado, USA) on a Zeiss Axio Observer 7 Advanced Marianas Z1 (Carl Zeiss AG, Oberkochen, Germany) inverted microscope equipped with Prime BSI Scientific sCMOS camera (Photometrics, Tucson, Arizona, USA), CSU-W1 spinning disk unit (Yokogawa Electric Corporation, Tokyo, Japan), and 3i solid state diode LaserStack. The images were acquired with a Zeiss Plan-Apochromat 63×/1.40 NA oil objective using the SlideBook program version 6.0. Z-stacks of 7–9 images with a slice thickness of 1 µm were collected using the top and bottom positions of the cells.

3D organoids were fixed with 2% PFA for 20 min at RT and thereafter washed with PBS. Organoids were permeabilized with 0.25% Triton X-100 in PBS for 10 min at +4°C, and thereafter washed with PBS. The non-specific binding sites were blocked in immunofluorescence (IF) buffer (0.2% Triton-X, 0.05% Tween 20, 0.1% BSA in PBS) supplemented with 10% normal goat serum (Gibco) for 1–2 h. The primary antibody (K8, Developmental Studies Hybridoma Bank TROMA-1, 1:300; K14, Santa Cruz Biotechnology 905301, 1:300; p21, Cell Signaling Technologies 2947, 1:300) was incubated in blocking solution (IF buffer with 10% normal goat serum) overnight at +4°C. Following the incubation, structures were washed three times with IF buffer, 15 min each wash, and then incubated with appropriate Alexa Fluor secondary antibody diluted in blocking solution. After 40–50 min incubation at RT, the structures were washed with IF buffer as before and the nuclei were counterstained with Hoechst 33342. All samples were mounted using Immu-Mount (Thermo Fisher Scientific) mounting reagent. Images were acquired using Leica TCS SP5 confocal microscope with HCX PL APO CS 63× glycerol (NA 1.3) objective, Leica SP8 Upright confocal with HC PL APO 63× CORR CS2 (NA 1.3), Leica TCS SP8 STED 3X CW 3D confocal with HC PL APO 63× water (NA 1.20) motCORR CS2 objective and LAS X software, or with Leica DM6000b widefield microscope with 20×/0.7 HC PL APO CS wd=0.59 objective and Hamamatsu Orca-Flash4.0 V2 sCMOS camera and LAS X software.

Internal reflection microscopy

To perform internal reflection microscopy (IRM), cells were seeded onto cell culture dishes coated with either 25 µg/ml laminin-111 or laminin-521 (BioLamina). To examine the immediate attachment kinetics and attachment surface area of cells, the time-lapse imaging was directly started after seeding of the cells. IRM can detect surface-to-surface contact, by measuring the interference patterns of light reflected from the slide–cell or slide–medium interfaces and therefore no staining was used. Imaging was performed on a Nikon A1R inverted point scanning confocal microscope using the 638.5 µm laser at a rate of 1 image per minute. The average cell attachment surface area was measured with Nikon Elements software.

Electron microscopy

Cells were processed for scanning electron microscopy (SEM) in the Electron Microscopy Unit of the Institute of Biotechnology at University of Helsinki. Cells were fixed with 2% glutaraldehyde in 100 mM sodium cacodylate (NaCac) buffer (pH 7.4) for 1–2 h at RT and washed subsequently twice with 0.1 M NaCac buffer 5 min each. Thereafter, samples were osmicated with 1% O_SO_4 in 0.1 M NaCac buffer for 1 h and washed twice with 0.1 M NaCac for 5 min each wash, and then three times with dH$_2$O 10 min each wash. Samples were then dehydrated and dried using methylhexadisilatzane (Fluka) overnight prior to platinum coating. SEM images were acquired using FEI Quanta 250 Field Emission Gun SEM.

Quantification of cell proliferation and growth

For quantification of cell proliferation, cells were seeded on laminin-coated coverslips and grown for 48 h, and thereafter treated with 10 µM 5-ethynyl-2′-deoxyuridine (EdU) for 2 h and fixed with 4% PFA. Immunostaining to detect EdU-positive cells was performed using the Click-IT EdU Alexa Fluor 647 Imaging Kit (Thermo Fisher Scientific) according to manufacturer's instructions. Before mounting, nuclei were counterstained

with Hoechst 33258 (Sigma). For quantification of cell growth, cells were seeded on laminin-coated multiwell plates and placed in a Cell-IQ (Chip-Man Technologies) cell culture platform. Cells from multiple locations within wells were imaged every 24 h. The cell number per timepoint was recorded from the images using Fiji software.

Quantification of apoptotic cells, and K8 and p21 positivity
Cells immunostained with antibody against cleaved caspase 3 or p21 were imaged with Leica DM6000b with 20x objective acquiring a 5X5 tile scan per sample. Tiles were stitched in the LAS X software, and the stitched images were opened in Tonga image analysis software (Ritchie et al., 2022) (https://github.com/avritchie/tonga). The number of cells and cells positive for cleaved caspase 3, K8 or p21 were quantified using the Count the ratio of positive nuclei protocol.

Analysis of HMEC population identities
The antibody-labeled cells were imaged with the same laser power and exposure times in all replicate experiments. Cell type categorization was done by visual scoring from merged maximum intensity projection images of ITGA6, EpCAM, and CD10 channels. Each cell was scored as high/low expression level for EpCAM and ITGA6, and positive/negative for CD10. The identification of luminal (EpCAM^{hi}/ITGA6^{low}/CD10^{neg}), basal (EpCAM^{low}/ITGA6^{hi}/CD10^{pos}), and stromal cells (EpCAM$^{low/neg}$/ITGA6^{hi}/CD10^{neg}) were based on previous publications (Linnemann et al., 2015; Moritani et al., 2002).

Wholemount staining
Mammary gland tissue samples for wholemount staining were fixed in 4% PFA overnight. For wholemount staining, #4 inguinal mammary glands were stained for several hours in carmine-alumn staining solution (2% w/v Carmine, Sigma; 5% w/v aluminium potassium sulfate, Sigma). After the desired color had developed, glands were mounted on to glass coverslips and imaged.

RNA isolation and quantitative PCR
RNA isolation was performed using RNeasy isolation kit (Qiagen) combined with On-Column DNase digestion (Qiagen) according to the manufacturer's instructions. cDNA synthesis was performed with Revert Aid cDNA synthesis kit (Thermo Fisher Scientific) starting with 500 ng of RNA. qPCR was performed with Power SYBR green master mix (Applied Biosystems) and a Bio-Rad CFX384 Touch Real-Time PCR detection system. Data was analyzed using BioRad CFX Manager program. Relative mRNA amounts were assayed by comparing PCR cycles to GAPDH using the ddCT method (Livak method) and normalizing to control samples. The following primers were used: hGAPDH fwd, 5′-AAGGTCGGAG-TCAACGGAT-3′, hGAPDH rev, 5′-TTGATGACAAGCTTCCCGTT-3′; hKRT8 fwd, 5′-CAGAAGTCCTACAAGGTGTCCA-3′, hKRT8 rev, 5′-CTCTGGTTGACCGTAACTGCG-3′ [Harvard Primer Bank (https://pga.mgh.harvard.edu/primerbank/) ID: 372466576c1]; hSEMA3B fwd, 5′-ACATTGGTACTGAGTGCATGAAC-3′, hSEMA3B rev, 5′-GCCATC-CTCTATCCTTCCTGG-3′ (Harvard Primer Bank ID: 54607087c1); hLAMA3 fwd, 5′-CACCGGGATATTTCGGGAATC-3′, hLAMA3 rev, 5′-AGCTGTCGCAATCATCACATT-3′ (Harvard Primer Bank ID: 189217424c1); hTP63 fwd, 5′-GGACCAGCAGATTCAGAACGG-3′, hTP63 rev, 5′-AGGACACGTCGAAACTGTGC-3′ (Harvard Primer Bank ID: 169234656c1); hKRT19 fwd, 5′-ACCAAGTTTGAGACGGAACAG-3′, hKRT19 rev, 5′-CCCTCAGCGTACTGATTTCCT-3′ (Harvard Primer Bank ID: 131412244c2); hSMA fwd, 5′-AAAAGACAGCTACGTGGGTGA-3′, hSMA rev, 5′-GCCATGTTCTATCGGGTACTTC-3′ (Harvard Primer Bank ID: 213688378c1); hCDKN1A fwd, 5′-CGATGGAACTTCGAC-TTTGTCA-3′, hCDKN1A rev, 5′-GCACAAGGGTACAAGACAGTG-3′ (Harvard Primer Bank ID: 310832423c2); mGAPDH fwd, 5′-AAGGT-CGGAGTCAACGGATT-3′, mGAPDH rev, 5′-TTGATGACAAGC-TTCCCGTT-3′, mKrt14 fwd, 5′-AGCGGCAAGAGTGAGATTTCT-3′, mKrt14 rev, 5′-CCTCCAGGTTATTCTCCAGGG-3′ (Harvard Primer Bank ID: 21489934c1); mKrt5 fwd, 5′-TCCAGTGTGTCCTTCCGAAGT-3′, mKrt5 rev, 5′-TGCCTCCGCCAGAACTGTA-3′ (Harvard Primer Bank ID: 118130335c1); mEzh2 fwd, 5′-AGCACAAGTCATCCCGTTAAAG-3′, mEzh2 rev, 5′-AATTCTGTTGTAAGGGCGACC-3′ (Harvard Primer Bank

ID: 226442806c1); mLama5 fwd, 5′-GGGTGGAGTTACTGAGTGCC-3′, mLama5 rev, AGCTACGGCAGCCAAAGTAG-3′.

RNA sequencing and data analysis
RNA was isolated using RNeasy isolation kit (Qiagen) as described above. Total RNA was subjected to quality control with Agilent Tapestation according to the manufacturer's instructions. To construct libraries suitable for Illumina sequencing, the Illumina TruSeq Stranded mRNA Sample preparation protocol, which includes mRNA extraction, cDNA synthesis, ligation of adapters and amplification of indexed libraries, was used. The yield and quality of the amplified libraries were analyzed using Qubit by Thermo Fisher Scientific and the Agilent TapeStation. The indexed cDNA libraries were next normalized and combined, and the pools were sequenced on the Illumina HiSeq 2000 for a 50-cycle v3 sequencing run generating 50 bp single-end reads. Basecalling and demultiplexing was performed using CASAVA software with default settings, generating Fastq files. The resulting Fastq files were passed to STAR for alignment to the human reference genome (hg38) and read counting of annotated genes. The reference genome and annotations were obtained from the UCSC (https://genome.ucsc.edu/). The gene counts were then imported to R/Bioconductor. Reads were trimmed mean of M values (TMM) normalized and analysis of differential gene expression was carried out with generalized linear models in EdgeR (McCarthy et al., 2012). For the analysis, only genes that had at least one count per million (CPM) in four or more samples were considered. Gene set enrichment analysis (GSEA) was carried out with default parameters using log2 fold change pre-ranked gene lists (all genes with >1 CPM) of LM-521 grown cells vs cells grown on uncoated dishes. Tested gene sets included gene sets upregulated and downregulated in basal HMECs and gene sets upregulated and downregulated in mammary stem cells [M5505 and M13422 (Huper and Marks, 2007); M2573 and M2574 (Lim et al., 2010), which are available from Molecular Signatures DataBase MSigDB (http://www.broad.mit.edu/gsea/.msigdb/msigdb_index.html)].

Plasmid construction for cDNA expression
PI3K H1047R cDNA in pBABEpuro retroviral vector was acquired from Addgene (plasmid #12524), PCR amplified (with following primers: PI3K-attB fwd 5′-GGGGACAACTTTGTACAAAAAAGTTGGCACCATGGG-GTACCCATACG-3′, PI3K-attB rev 5′-GGGGACAACTTTGTACAAG-AAAGTTGGCAATCAGTTCAATGCATGCTGT-3′) and ligated into pDONR21 vector in Genome Biology Unit (GBU) cloning service at University of Helsinki. Next, PI3K H1047R was transferred into pLEX_307 (Addgene plasmid #41392) vector using a standard Gateway LR clonase protocol. eGFP from the Human ORFeome collaboration library at GBU was similarly cloned to pLEX_307 and used as a control. Plasmids were verified by sequencing.

Plasmid construction for CRISPR guides
CRISPR guides were designed to target ITGB4 using the CRISPR Design tool (http://crispr.mit.edu). The following target sequences were used: gITGB4: 5′-GTGCAGGCTGGTGTCGATCT-3′; gSCRA: 5′-CTA-AAACTGCGGATACAATC-3′. Oligonucleotides with target sequences were designed according to published instructions (Shalem et al., 2014), annealed and cloned into the pLentiCRISPRv2 vector (Addgene plasmid #52961; deposited by Feng Zhang).

Lentiviral virus production and infection
Lentiviruses were produced in 293fT cells (Thermo Fisher Scientific) grown in DMEM (Sigma) supplemented with 10% FCS (Gibco), penicillin-streptomycin (Orion and Sigma) and 2 mM glutamine (Sigma). Transfections of transfer vector (pLEX_307 PI3K H1047R, pLEX_307 eGFP, pLentiCRISPRv2 gITGB4 and pLentiCRISPRv2g SCRA) and packaging plasmids (CMV-VSVg and Delta8.9) were performed using Lipofectamine 2000 (Invitrogen) according to manufacturer's instructions. Virus-containing supernatant was collected from transfected cells 72 h post-transfection and filtered through 0.45 µM PES-filter. To produce stable cell lines, cells were incubated with freshly collected viral supernatant on 6-well plates for 6–8 h, whereafter medium was changed to the normal growth

media of cells. Puromycin (Sigma) was added at 2 μg/ml concentration at 48 h after the infection to select cells.

Western blotting

Cells were lysed with radioimmunoprecipitation assay (RIPA) buffer (150 mM NaCl, 20 mM Tris-HCl pH 7.5, 0.1% SDS, 1.0% sodium deoxycholate and 0.1% Triton X-100; all from Sigma) supplemented with EDTA-free protease inhibitor cocktail (Roche). Lysates were incubated on ice for 10 min and thereafter cleared by centrifugation at 13,000 g at +4°C for 15 min. Protein concentration of cell lysates was determined using Bio-Rad protein assay (Bio-Rad). 20-40 μg samples were denatured with 5x Bolt sample buffer (Invitrogen) and separated in 4-12% Bis-Tris Plus Gels (Invitrogen), and subsequently transferred to nitrocellulose filters (Bio-Rad). Filters were blocked with 5% non-fat milk, 0.1% BSA and 0.1% Tween-20 (Sigma) in TBS and primary antibodies (β1-integrin, Abcam ab24693, 1:1000; β4-integrin, Abcam ab29042, 1:1000; p-AKT T308, Cell Signaling 13038, 1:1000; AKT, Cell Signaling 9272, 1:1000; PI3K p110, Cell Signaling 4249, 1:500; p53, Santa Cruz Biotechnology sc-126, 1:500; β-actin, Cell Signaling 4967, 1:2000; GAPDH, Cell Signaling 2118, 1:2000) were incubated overnight in the blocking solution. Antigen detection was performed with specific HRP-conjugated antibodies (anti-rabbit IgG-HRP or anti-mouse IgG-HRP, 1:1000) and SuperSignal West Femto Maximum Sensitivity Substrate (Pierce). Western blotting quantification was performed in Fiji/ImageJ 2 version 2.3.0/1.53q using the analyze gels tool. Full images of western blots are given in Fig. S7.

Quantification and statistical analysis

Data is presented as mean±s.d. or s.e.m. from at least three independent experiments, unless otherwise stated in the figure legend. Unpaired two-tailed Student's t-tests were used to compare two groups, and one-way ANOVA with Tukey's multiple comparison test when compared to three or more groups. Statistical tests were performed using GraphPad Prism 9.

Data availability

RNA-seq data has been deposited to GEO with the accession #GSE197950.

Peer review history

The peer review history is available online at https://journals.biologists.com/jcs/lookup/doi/10.1242/jcs.260232.reviewer-comments.pdf

References

Asselin-Labat, M.-L., Vaillant, F., Sheridan, J. M., Pal, B., Wu, D., Simpson, E. R., Yasuda, H., Smyth, G. K., Martin, T. J., Lindeman, G. J. et al. (2010). Control of mammary stem cell function by steroid hormone signalling. *Nature* **465**, 798-802. doi:10.1038/nature09027

Barr, V. A. and Bunnell, S. C. (2009). Interference reflection microscopy. *Curr. Protoc. Cell Biol.* Chapter 4, Unit 4 23. doi:10.1002/0471143030.cb0423s45.

Cai, C., Yu, Q. C., Jiang, W., Liu, W., Song, W., Yu, H., Zhang, L., Yang, Y. and Zeng, Y. A. (2014). R-spondin1 is a novel hormone mediator for mammary stem cell self-renewal. *Genes Dev.* **28**, 2205-2218. doi:10.1101/gad.245142.114

Cai, S., Kalisky, T., Sahoo, D., Dalerba, P., Feng, W., Lin, Y., Qian, D., Kong, A., Yu, J., Wang, F. et al. (2017). A quiescent Bcl11b high stem cell population is required for maintenance of the mammary gland. *Cell Stem Cell* **20**, 247-260.e5. doi:10.1016/j.stem.2016.11.007

Centonze, A., Lin, S., Tika, E., Sifrim, A., Fioramonti, M., Malfait, M., Song, Y., Wuidart, A., Van Herck, J., Dannau, A. et al. (2020). Heterotypic cell-cell communication regulates glandular stem cell multipotency. *Nature* **584**, 608-613. doi:10.1038/s41586-020-2632-y

Chaffer, C. L., Brueckmann, I., Scheel, C., Kaestli, A. J., Wiggins, P. A., Rodrigues, L. O., Brooks, M., Reinhardt, F., Su, Y., Polyak, K. et al. (2011). Normal and neoplastic nonstem cells can spontaneously convert to a stem-like state. *Proc. Natl. Acad. Sci. USA* **108**, 7950-7955. doi:10.1073/pnas.1102454108

Cheng, T., Rodrigues, N., Shen, H., Yang, Y., Dombkowski, D., Sykes, M. and Scadden, D. T. (2000). Hematopoietic stem cell quiescence maintained by p21cip1/waf1. *Science* **287**, 1804-1808. doi:10.1126/science.287.5459.1804

Chiche, A., Moumen, M., Petit, V., Jonkers, J., Medina, D., Deugnier, M.-A., Faraldo, M. M. and Glukhova, M. A. (2013). Somatic loss of p53 leads to stem/progenitor cell amplification in both mammary epithelial compartments, basal and luminal. *Stem Cells* **31**, 1857-1867. doi:10.1002/stem.1429

Cicalese, A., Bonizzi, G., Pasi, C. E., Faretta, M., Ronzoni, S., Giulini, B., Brisken, C., Minucci, S., Di Fiore, P. P. and Pelicci, P. G. (2009). The tumor suppressor p53 regulates polarity of self-renewing divisions in mammary stem cells. *Cell* **138**, 1083-1095. doi:10.1016/j.cell.2009.06.048

Clarke, A. S., Lotz, M. M., Chao, C. and Mercurio, A. M. (1995). Activation of the p21 pathway of growth arrest and apoptosis by the β4 integrin cytoplasmic domain. *J. Biol. Chem.* **270**, 22673-22676. doi:10.1074/jbc.270.39.22673

Dontu, G., Abdallah, W. M., Foley, J. M., Jackson, K. W., Clarke, M. F., Kawamura, M. J. and Wicha, M. S. (2003). In vitro propagation and transcriptional profiling of human mammary stem/progenitor cells. *Genes Dev.* **17**, 1253-1270. doi:10.1101/gad.1061803

Englund, J. I., Ritchie, A., Blaas, L., Cojoc, H., Pentinmikko, N., Döhla, J., Iqbal, S., Patarroyo, M. and Katajisto, P. (2021). Laminin alpha 5 regulates mammary gland remodeling through luminal cell differentiation and Wnt4-mediated epithelial crosstalk. *Development* **148**, dev199281. doi:10.1242/dev.199281

Feng, Y., Manka, D., Wagner, K.-U. and Khan, S. A. (2007). Estrogen receptor-α expression in the mammary epithelium is required for ductal and alveolar morphogenesis in mice. *Proc. Natl. Acad. Sci. USA* **104**, 14718-14723. doi:10.1073/pnas.0706933104

Forster, N., Saladi, S. V., van Bragt, M., Sfondouris, M. E., Jones, F. E., Li, Z. and Ellisen, L. W. (2014). Basal cell signaling by p63 controls luminal progenitor function and lactation via NRG1. *Dev. Cell* **28**, 147-160. doi:10.1016/j.devcel.2013.11.019

Ge, Y., Gomez, N. C., Adam, R. C., Nikolova, M., Yang, H., Verma, A., Lu, C. P.-J., Polak, L., Yuan, S., Elemento, O. et al. (2017). Stem cell lineage infidelity drives wound repair and cancer. *Cell* **169**, 636-650.e14. doi:10.1016/j.cell.2017.03.042

Gudjonsson, T., Rønnov-Jessen, L., Villadsen, R., Rank, F., Bissell, M. J. and Petersen, O. W. (2002). Normal and tumor-derived myoepithelial cells differ in their ability to interact with luminal breast epithelial cells for polarity and basement membrane deposition. *J. Cell Sci.* **115**, 39-50. doi:10.1242/jcs.115.1.39

Guo, W., Pylayeva, Y., Pepe, A., Yoshioka, T., Muller, W. J., Inghirami, G. and Giancotti, F. G. (2006). β4 integrin amplifies ErbB2 signaling to promote mammary tumorigenesis. *Cell* **126**, 489-502. doi:10.1016/j.cell.2006.05.047

Hemmings, B. A. and Restuccia, D. F. (2012). PI3K-PKB/Akt pathway. *Cold Spring Harb. Perspect. Biol.* **4**, a011189. doi:10.1101/cshperspect.a011189

Hu, Y. and Smyth, G. K. (2009). ELDA: extreme limiting dilution analysis for comparing depleted and enriched populations in stem cell and other assays. *J. Immunol. Methods* **347**, 70-78. doi:10.1016/j.jim.2009.06.008

Huper, G. and Marks, J. R. (2007). Isogenic normal basal and luminal mammary epithelial isolated by a novel method show a differential response to ionizing radiation. *Cancer Res.* **67**, 2990-3001. doi:10.1158/0008-5472.CAN-06-4065

Inman, J. L., Robertson, C., Mott, J. D. and Bissell, M. J. (2015). Mammary gland development: cell fate specification, stem cells and the microenvironment. *Development* **142**, 1028-1042. doi:10.1242/dev.087643

Jamieson, P. R., Dekkers, J. F., Rios, A. C., Fu, N. Y., Lindeman, G. J. and Visvader, J. E. (2017). Derivation of a robust mouse mammary organoid system for studying tissue dynamics. *Development* **144**, 1065-1071. doi:10.1242/dev.145045

Katajisto, P., Döhla, J., Chaffer, C. L., Pentinmikko, N., Marjanovic, N., Iqbal, S., Zoncu, R., Chen, W., Weinberg, R. A. and Sabatini, D. M. (2015). Stem cells. Asymmetric apportioning of aged mitochondria between daughter cells is required for stemness. *Science* **348**, 340-343. doi:10.1126/science.1260384

Klinowska, T. C. M., Alexander, C. M., Georges-Labouesse, E., Van der Neut, R., Kreidberg, J. A., Jones, C. J. P., Sonnenberg, A. and Streuli, C. H. (2001).

Epithelial development and differentiation in the mammary gland is not dependent on α3 or α6 integrin subunits. *Dev. Biol.* **233**, 449-467. doi:10.1006/dbio.2001.0204

Koren, S., Reavie, L., Couto, J. P., De Silva, D., Stadler, M. B., Roloff, T., Britschgi, A., Eichlisberger, T., Kohler, H., Aina, O. et al. (2015). PIK3CA(H1047R) induces multipotency and multi-lineage mammary tumours. *Nature* **525**, 114-118. doi:10.1038/nature14669

LaBarge, M. A., Nelson, C. M., Villadsen, R., Fridriksdottir, A., Ruth, J. R., Stampfer, M. R., Petersen, O. W. and Bissell, M. J. (2009). Human mammary progenitor cell fate decisions are products of interactions with combinatorial microenvironments. *Integr. Biol.* **1**, 70-79. doi:10.1039/B816472J

Li, N., Zhang, Y., Naylor, M. J., Schatzmann, F., Maurer, F., Wintermantel, T., Schuetz, G., Mueller, U., Streuli, C. H. and Hynes, N. E. (2005). β1 integrins regulate mammary gland proliferation and maintain the integrity of mammary alveoli. *EMBO J.* **24**, 1942-1953. doi:10.1038/sj.emboj.7600674

Li, J., Sun, H., Feltri, M. L. and Mercurio, A. M. (2015). Integrin β4 regulation of PTHrP underlies its contribution to mammary gland development. *Dev. Biol.* **407**, 313-320. doi:10.1016/j.ydbio.2015.09.015

Lilja, A. M., Rodilla, V., Huyghe, M., Hannezo, E., Landragin, C., Renaud, O., Leroy, O., Rulands, S., Simons, B. D. and Fre, S. (2018). Clonal analysis of Notch1-expressing cells reveals the existence of unipotent stem cells that retain long-term plasticity in the embryonic mammary gland. *Nat. Cell Biol.* **20**, 677-687. doi:10.1038/s41556-018-0108-1

Lim, E., Wu, D., Pal, B., Bouras, T., Asselin-Labat, M.-L., Vaillant, F., Yagita, H., Lindeman, G. J., Smyth, G. K. and Visvader, J. E. (2010). Transcriptome analyses of mouse and human mammary cell subpopulations reveal multiple conserved genes and pathways. *Breast Cancer Res.* **12**, R21. doi:10.1186/bcr2560

Linnemann, J. R., Miura, H., Meixner, L. K., Irmler, M., Kloos, U. J., Hirschi, B., Bartsch, H. S., Sass, S., Beckers, J., Theis, F. J. et al. (2015). Quantification of regenerative potential in primary human mammary epithelial cells. *Development* **142**, 3239-3251. doi:10.1242/dev.123554

Linnemann, J. R., Meixner, L. K., Miura, H. and Scheel, C. H. (2017). An organotypic 3D assay for primary human mammary epithelial cells that recapitulates branching morphogenesis. *Methods Mol. Biol.* **1612**, 125-137. doi:10.1007/978-1-4939-7021-6_9

Macias, H. and Hinck, L. (2012). Mammary gland development. *Wiley Interdiscip. Rev. Dev. Biol.* **1**, 533-557. doi:10.1002/wdev.35

Maller, O., Martinson, H. and Schedin, P. (2010). Extracellular matrix composition reveals complex and dynamic stromal-epithelial interactions in the mammary gland. *J. Mammary Gland Biol. Neoplasia* **15**, 301-318. doi:10.1007/s10911-010-9189-6

Margueron, R. and Reinberg, D. (2011). The Polycomb complex PRC2 and its mark in life. *Nature* **469**, 343-349. doi:10.1038/nature09784

Marqués-Torrejón, M. A., Porlan, E., Banito, A., Gomez-Ibarlucea, E., Lopez-Contreras, A. J., Fernandez-Capetillo, O., Vidal, A., Gil, J., Torres, J. and Farinas, I. (2013). Cyclin-dependent kinase inhibitor p21 controls adult neural stem cell expansion by regulating Sox2 gene expression. *Cell Stem Cell* **12**, 88-100. doi:10.1016/j.stem.2012.12.001

McCarthy, D. J., Chen, Y. and Smyth, G. K. (2012). Differential expression analysis of multifactor RNA-Seq experiments with respect to biological variation. *Nucleic Acids Res.* **40**, 4288-4297. doi:10.1093/nar/gks042

Moritani, S., Kushima, R., Sugihara, H., Bamba, M., Kobayashi, T. K. and Hattori, T. (2002). Availability of CD10 immunohistochemistry as a marker of breast myoepithelial cells on paraffin sections. *Mod. Pathol.* **15**, 397-405. doi:10.1038/modpathol.3880536

Murgia, C., Blaikie, P., Kim, N., Dans, M., Petrie, H. T. and Giancotti, F. G. (1998). Cell cycle and adhesion defects in mice carrying a targeted deletion of the integrin β4 cytoplasmic domain. *EMBO J.* **17**, 3940-3951. doi:10.1093/emboj/17.14.3940

Naylor, M. J., Li, N., Cheung, J., Lowe, E. T., Lambert, E., Marlow, R., Wang, P., Schatzmann, F., Wintermantel, T., Schüetz, G. et al. (2005). Ablation of β1 integrin in mammary epithelium reveals a key role for integrin in glandular morphogenesis and differentiation. *J. Cell Biol.* **171**, 717-728. doi:10.1083/jcb.200503144

Nerger, B. A., Jaslove, J. M., Elashal, H. E., Mao, S., Košmrlj, A., Link, A. J. and Nelson, C. M. (2021). Local accumulation of extracellular matrix regulates global morphogenetic patterning in the developing mammary gland. *Curr. Biol.* **31**, 1903-1917.e6. doi:10.1016/j.cub.2021.02.015

Nguyen, N. M., Kelley, D. G., Schlueter, J. A., Meyer, M. J., Senior, R. M. and Miner, J. H. (2005). Epithelial laminin α5 is necessary for distal epithelial cell maturation, VEGF production, and alveolization in the developing murine lung. *Dev. Biol.* **282**, 111-125. doi:10.1016/j.ydbio.2005.02.031

Olabi, S., Ucar, A., Brennan, K. and Streuli, C. H. (2018). Integrin-Rac signalling for mammary epithelial stem cell self-renewal. *Breast Cancer Res.* **20**, 128. doi:10.1186/s13058-018-1048-1

Pal, B., Chen, Y., Vaillant, F., Jamieson, P., Gordon, L., Rios, A. C., Wilcox, S., Fu, N., Liu, K. H., Jackling, F. C. et al. (2017). Construction of developmental lineage relationships in the mouse mammary gland by single-cell RNA profiling. *Nat. Commun.* **8**, 1627. doi:10.1038/s41467-017-01560-x

Rajaram, R. D., Buric, D., Caikovski, M., Ayyanan, A., Rougemont, J., Shan, J., Vainio, S. J., Yalcin-Ozuysal, O. and Brisken, C. (2015). Progesterone and Wnt4 control mammary stem cells via myoepithelial crosstalk. *EMBO J.* **34**, 641-652. doi:10.15252/embj.201490434

Ramovs, V., Te Molder, L. and Sonnenberg, A. (2017). The opposing roles of laminin-binding integrins in cancer. *Matrix Biol.* **57-58**, 213-243. doi:10.1016/j.matbio.2016.08.007

Ritchie, A., Laitinen, S., Katajisto, P. and Englund, J. (2022). "Tonga": a novel toolbox for straightforward bioimage analysis. *Front. Comput. Sci.* **4**, 777458. doi:10.3389/fcomp.2022.777458

Rodin, S., Antonsson, L., Hovatta, O. and Tryggvason, K. (2014). Monolayer culturing and cloning of human pluripotent stem cells on laminin-521-based matrices under xeno-free and chemically defined conditions. *Nat. Protoc.* **9**, 2354-2368. doi:10.1038/nprot.2014.159

Romagnoli, M., Cagnet, S., Chiche, A., Bresson, L., Baulande, S., de la Grange, P., De Arcangelis, A., Kreft, M., Georges-Labouesse, E., Sonnenberg, A. et al. (2019). Deciphering the mammary stem cell niche: a role for laminin-binding integrins. *Stem Cell Reports* **12**, 831-844. doi:10.1016/j.stemcr.2019.02.008

Romagnoli, M., Bresson, L., Di-Cicco, A., Pérez-Lanzón, M., Legoix, P., Baulande, S., de la Grange, P., De Arcangelis, A., Georges-Labouesse, E., Sonnenberg, A. et al. (2020). Laminin-binding integrins are essential for the maintenance of functional mammary secretory epithelium in lactation. *Development* **147**, dev181552. doi:10.1242/dev.181552

Seldin, L. and Macara, I. G. (2020). DNA damage promotes epithelial hyperplasia and fate mis-specification via fibroblast inflammasome activation. *Dev. Cell* **55**, 558-573.e6. doi:10.1016/j.devcel.2020.09.021

Shackleton, M., Vaillant, F., Simpson, K. J., Stingl, J., Smyth, G. K., Asselin-Labat, M.-L., Wu, L., Lindeman, G. J. and Visvader, J. E. (2006). Generation of a functional mammary gland from a single stem cell. *Nature* **439**, 84-88. doi:10.1038/nature04372

Shalem, O., Sanjana, N. E., Hartenian, E., Shi, X., Scott, D. A., Mikkelson, T. S., Heckl, D., Ebert, B. L., Root, D. E., Doench, J. G. et al. (2014). Genome-scale CRISPR-Cas9 knockout screening in human cells. *Science* **343**, 84-87. doi:10.1126/science.1247005

Shaw, F. L., Harrison, H., Spence, K., Ablett, M. P., Simões, B. M., Farnie, G. and Clarke, R. B. (2012). A detailed mammosphere assay protocol for the quantification of breast stem cell activity. *J. Mammary Gland Biol. Neoplasia* **17**, 111-117. doi:10.1007/s10911-012-9255-3

Stingl, J., Eirew, P., Ricketson, I., Shackleton, M., Vaillant, F., Choi, D., Li, H. I. and Eaves, C. J. (2006). Purification and unique properties of mammary epithelial stem cells. *Nature* **439**, 993-997. doi:10.1038/nature04496

Subramanian, A., Tamayo, P., Mootha, V. K., Mukherjee, S., Ebert, B. L., Gillette, M. A., Paulovich, A., Pomeroy, S. L., Golub, T. R., Lander, E. S. et al. (2005). Gene set enrichment analysis: a knowledge-based approach for interpreting genome-wide expression profiles. *Proc. Natl. Acad. Sci. USA* **102**, 15545-15550. doi:10.1073/pnas.0506580102

Taddei, I., Deugnier, M.-A., Faraldo, M. M., Petit, V., Bouvard, D., Medina, D., Fässler, R., Thiery, J. P. and Glukhova, M. A. (2008). β1 integrin deletion from the basal compartment of the mammary epithelium affects stem cells. *Nat. Cell Biol.* **10**, 716-722. doi:10.1038/ncb1734

Tomaselli, K. J., Damsky, C. H. and Reichardt, L. F. (1988). Purification and characterization of mammalian integrins expressed by a rat neuronal cell line (PC12): evidence that they function as α/β heterodimeric receptors for laminin and type IV collagen. *J. Cell Biol.* **107**, 1241-1252. doi:10.1083/jcb.107.3.1241

Van Keymeulen, A., Rocha, A. S., Ousset, M., Beck, B., Bouvencourt, G., Rock, J., Sharma, N., Dekoninck, S. and Blanpain, C. (2011). Distinct stem cells contribute to mammary gland development and maintenance. *Nature* **479**, 189-193. doi:10.1038/nature10573

Vassilev, L. T., Vu, B. T., Graves, B., Carvajal, D., Podlaski, F., Filipovic, Z., Kong, N., Kammlott, U., Lukacs, C., Klein, C. et al. (2004). In vivo activation of the p53 pathway by small-molecule antagonists of MDM2. *Science* **303**, 844-848. doi:10.1126/science.1092447

Wang, S., Matsumoto, K., Lish, S. R., Cartagena-Rivera, A. X. and Yamada, K. M. (2021). Budding epithelial morphogenesis driven by cell-matrix versus cell-cell adhesion. *Cell* **184**, 3702-3716.e30. doi:10.1016/j.cell.2021.05.015

Welm, B. E., Dijkgraaf, G. J. P., Bledau, A. S., Welm, A. L. and Werb, Z. (2008). Lentiviral transduction of mammary stem cells for analysis of gene function during development and cancer. *Cell Stem Cell* **2**, 90-102. doi:10.1016/j.stem.2007.10.002

Wuidart, A., Sifrim, A., Fioramonti, M., Matsumura, S., Brisebarre, A., Brown, D., Centonze, A., Dannau, A., Dubois, C., Van Keymeulen, A. et al. (2018). Early lineage segregation of multipotent embryonic mammary gland progenitors. *Nat. Cell Biol.* **20**, 666-676. doi:10.1038/s41556-018-0095-2

Yang, X., Pursell, B., Lu, S., Chang, T.-K. and Mercurio, A. M. (2009). Regulation of β4-integrin expression by epigenetic modifications in the mammary gland and during the epithelial-to-mesenchymal transition. *J. Cell Sci.* **122**, 2473-2480. doi:10.1242/jcs.049148

Yurchenco, P. D. (2011). Basement membranes: cell scaffoldings and signaling platforms. *Cold Spring Harb. Perspect. Biol.* **3**, a004911. doi:10.1101/cshperspect.a004911